Article

Cancer Cell

RORC1 Regulates Tumor-Promoting "Emergency" Granulo-Monocytopoiesis

Graphical Abstract

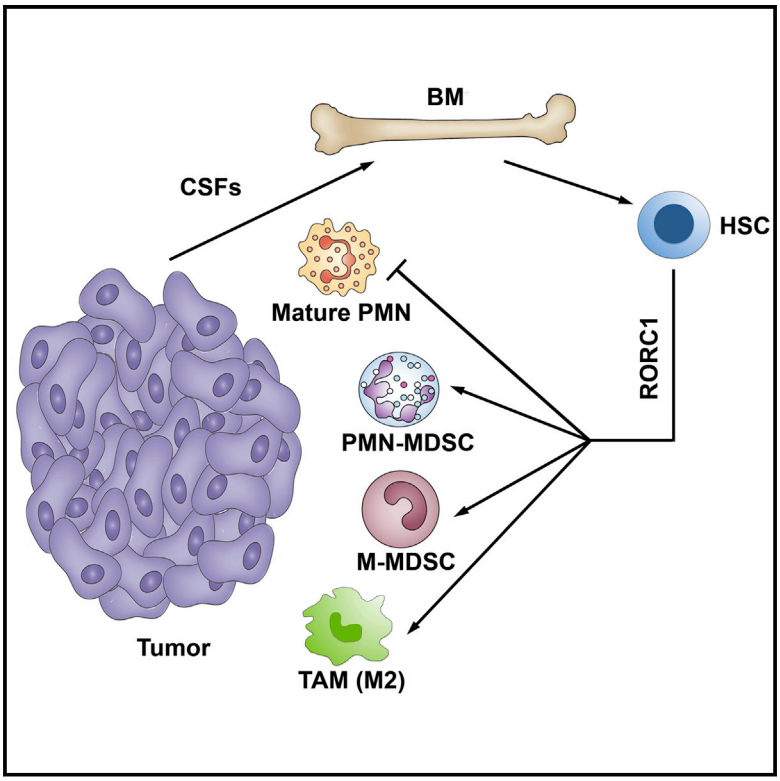

Authors

Laura Strauss, Sabina Sangaletti, Francesca Maria Consonni, ..., Claudio Tripodo, Mario P. Colombo, Antonio Sica

Correspondence

antonio.sica@humanitasresearch.it

In Brief

Strauss et al. show that RORC1 orchestrates myelopoiesis and supports tumor-promoting innate immunity. Importantly, ablation of RORC1 in the myeloid compartment inhibits tumor growth and metastasis, suggesting a cancer therapeutic approach.

Highlights

- RORC1 drives cancer-related myelopoiesis in response to colony-stimulating factors
- RORC1^{+} myeloid cells are a hallmark of tumor-promoting emergency myelopoiesis
- RORC1 ablation in the hematopoietic compartment prevents generation of MDSCs and TAMs
- RORC1 ablation in the hematopoietic compartment prevents tumor development

Strauss et al., 2015, Cancer Cell *28*, 253–269
August 10, 2015 ©2015 Elsevier Inc.
http://dx.doi.org/10.1016/j.ccell.2015.07.006

Cancer Cell
Article

RORC1 Regulates Tumor-Promoting "Emergency" Granulo-Monocytopoiesis

Laura Strauss,[1] Sabina Sangaletti,[4] Francesca Maria Consonni,[2] Gabor Szebeni,[1] Sara Morlacchi,[1] Maria Grazia Totaro,[1] Chiara Porta,[2] Achille Anselmo,[1] Silvia Tartari,[1] Andrea Doni,[1] Francesco Zitelli,[2] Claudio Tripodo,[3] Mario P. Colombo,[4] and Antonio Sica[1,2,*]

[1]Department of Inflammation and Immunology, Humanitas Clinical and Research Center, 20089 Rozzano, Milan, Italy
[2]Department of Pharmaceutical Sciences, Università del Piemonte Orientale "Amedeo Avogadro," Via Bovio 6, 28100 Novara, Italy
[3]Tumor Immunology Unit, Department of Health Sciences, University of Palermo, Via del Vespro 129, 90127 Palermo, Italy
[4]Experimental Oncology, Fondazione IRCCS Istituto Nazionale Tumori, 20133 Milan, Italy
*Correspondence: antonio.sica@humanitasresearch.it
http://dx.doi.org/10.1016/j.ccell.2015.07.006

SUMMARY

Cancer-driven granulo-monocytopoiesis stimulates expansion of tumor promoting myeloid populations, mostly myeloid-derived suppressor cells (MDSCs) and tumor-associated macrophages (TAMs). We identified subsets of MDSCs and TAMs based on the expression of retinoic-acid-related orphan receptor (RORC1/RORγ) in human and mouse tumor bearers. RORC1 orchestrates myelopoiesis by suppressing negative (Socs3 and Bcl3) and promoting positive (C/EBPβ) regulators of granulopoiesis, as well as the key transcriptional mediators of myeloid progenitor commitment and differentiation to the monocytic/macrophage lineage (IRF8 and PU.1). RORC1 supported tumor-promoting innate immunity by protecting MDSCs from apoptosis, mediating TAM differentiation and M2 polarization, and limiting tumor infiltration by mature neutrophils. Accordingly, ablation of RORC1 in the hematopoietic compartment prevented cancer-driven myelopoiesis, resulting in inhibition of tumor growth and metastasis.

INTRODUCTION

Immunologic stress, such as infection and cancer, modifies the magnitude and composition of the hematopoietic output, a feature of immune regulation defined as "emergency" hematopoiesis, to guarantee proper supply of immune cells to increased demand (Ueha et al., 2011). Tumors can reprogram myeloid cells to promote disease progression (Sica and Bronte, 2007). However, the molecular pathways guiding cancer-driven "emergency" myelopoiesis remain largely unknown. Colony-stimulating factors (CSFs) are major orchestrators of hematopoietic development. Among these, granulocyte CSF (G-CSF) and granulocyte-macrophage CSF (GM-CSF) drive "emergency" myelopoiesis by securing supply of neutrophils and macrophages from bone marrow (BM) and hematopoietic stem cell niches (HSCs) (Metcalf, 2008; Ueha et al., 2011). Further, the macrophage CSF (M-CSF) promotes macrophage differentiation from medullar precursors and differentiation of tissue macrophages involved in tissue homeostasis (Hume and MacDonald, 2012) and tumor progression (Qian and Pollard, 2010). Recent studies reveal that monocytic and granulocytic myeloid-derived suppressor cells (M-MDSCs and PMN-MDSCs, respectively) and tumor-associated macrophages (TAMs), the major myeloid populations associated with cancer development (Sica and Bronte, 2007), differentiate from a common myeloid progenitor (CMP) (Gabrilovich et al., 2012). Importantly, reciprocal regulation of macrophage versus neutrophil/granulocyte differentiation might control tissue homeostasis. Depletion of tissue macrophages leads to exacerbated G-CSF-mediated granulopoiesis (Gordy et al., 2011; Goren et al., 2009), and tissue macrophages

Significance

Preclinical data show that MDSCs and TAMs orchestrate tumor-promoting conditions, suggesting these cells as attractive therapeutic targets. MDSC and TAM generation is tightly associated with the altered hematopoietic output that occurs in cancer, defined as "emergency hematopoiesis." Here we report that RORC1 is a key driver of emergency hematopoiesis in tumor bearers, in response to colony-stimulating factors (G-CSF, GM-CSF, and M-CSF), and that RORC1-expressing myeloid cells mark advanced cancer inflammation. We demonstrate that ablation of RORC1 in the myeloid compartment impairs tumor development and the generation of suppressive MDSCs while promoting generation of antitumor M1-polarized TAMs. Thus, inhibition of RORC1-dependent myelopoiesis may represent a therapeutic approach to prevent the induction of the tumor-promoting host macro- and micro-environments.

regulate HSC niche homeostasis (Chow et al., 2011; Winkler et al., 2010). Thus, investigation of the molecular networks that dictate this reciprocal regulation appears to be crucial, as it may affect tissue homeostasis during cancerogenesis.

G-CSF-induced granulopoiesis is mediated through the transcription factors c-EBPβ (Akagi et al., 2008) and STAT3 (Zhang et al., 2010), whereas M-CSF supports monocyte differentiation through the transcription factors PU.1 and IRF8 (Friedman, 2007). Of relevance, interleukin-17A (IL-17A) promotes G-CSF- and stem-cell-factor-mediated neutrophilia (Liu et al., 2010) and supports G-CSF-driven "emergency" myelopoiesis (Schwarzenberger et al., 2000).

Despite the fact that IL-17 expression in cancer has been so far mainly restricted to the adaptive immunity (Iwakura et al., 2011) and its role in cancer remains controversial (Toomer and Chen, 2014), TAMs and MDSCs produce the Th17-driving cytokines TGFβ and IL-6 (Zamarron and Chen, 2011), and IL-17-expressing cells with macrophage morphology have been described in cancer patients (Zhu et al., 2008). Although the Th17 response is controlled by the orphan nuclear receptor retinoic-acid-related orphan receptor gamma (RORγ) full-length protein (RORC1) and the RORCγt splice variant (RORC2) (Ivanov et al., 2006), the signaling pathways that drive IL-17-producing innate immune cells have been poorly investigated. IL-17A-expressing myeloid cells have been reported in inflammation (Taylor et al., 2014; Zhu et al., 2008; Zhuang et al., 2012). In arthritis patients, mast cells express a dual RORC1/IL-17A fingerprint in response to TLR4 ligands (Hueber et al., 2010), and a population of RORγt-expressing neutrophils that produce IL-17 was identified in fungal infection (Taylor et al., 2014). We explored the role of the IL-17/RORC1 axis in myeloid lineage differentiation and commitment associated with cancer development.

RESULTS

Divergent RORC1/IL-17A Fingerprint in Tumor-Associated Myeloid Cells

To clarify the role of IL-17A$^+$ innate immune cells in tumor progression, we screened the myeloid compartment of fibrosarcoma (MN/MCA1)-bearing C57BL/6 mice. A tumor volume of <1.5 cm^3 and few lung metastases (fewer than five), at days 21–23 after tumor cell injection, was defined as early-stage disease (ED), whereas tumors larger than 2 cm^3 and a higher number of lung metastases (more than 15; days 25–28) was defined as advanced-stage disease (AD) (Figure S1). In AD, few blood and spleen CD45$^+$CD3$^+$ T cells expressed IL-17A (data not shown), whereas IL-17A was significantly expressed by CD45$^+$CD3$^-$ cells in the blood (30% ± 3%) and spleen (12% ± 1.5%) (Figure 1A). Few CD45$^+$CD3$^-$ cells expressed IL-17A in non-tumor bearers (NTs) and ED, suggesting that IL-17A$^+$ myeloid cells mark advanced cancer-associated inflammation. FACS analysis of the CD45$^+$CD3$^-$ cell pool confirmed that Gr1$^+$CD11b$^+$ MDSCs represent the major splenic myeloid population in AD (Figure 1B), comprising a predominant polymorphonuclear CD11b$^+$Gr1$^+$Ly6G^{high}Ly6C^{low} (PMN-MDSC) population and side monocytic CD11b$^+$Gr1$^+$Ly6C^{high}Ly6G^{low} (M-MDSC) and CD11b$^+$F4/80$^+$ macrophage populations. IL-17A was significantly expressed by PMN-MDSCs in the blood and spleen of AD mice (Figure 1C), although these cells failed to release IL-17 in response to degranulating signals, including CD16/32 (FCII/III) antibody-mediated cross-linkage and C5a (data not shown) (Mantovani et al., 2011). In contrast, IL-17A was poorly or not expressed by M-MDSCs (Figure 1C) and CD11b$^+$F4/80$^+$ macrophages (data not shown). RORC1 and its splice variant RORC2 are master regulators of IL-17A gene transcription in Th17 cells (Ivanov et al., 2006), innate lymphocytes (Sawa et al., 2010), γδ T cells (Gray et al., 2011), and natural killer T cells (Rachitskaya et al., 2008). Hence, we tested by FACS whether IL-17 expression in myeloid cells was associated with RORC1. In keeping with IL-17A expression, the majority of blood and spleen PMN-MDSCs from AD mice expressed RORC1, while its expression was restricted to a minor subset of IL-17A$^-$ M-MDSCs (Figure 1D, left). Nevertheless, as compared to PMN-MDSCs, M-MDSCs expressed higher levels of RORC1, estimated as mean fluorescence intensity (MFI) (Figure 1D, right). It is noteworthy that RORC1 was highly expressed by splenic IL-17A$^-$CD11b$^+$F4/80$^+$ macrophages in AD mice (Figure 1E), by F4/80$^+$ TAMs (>90%) and thyoglicollate-elicited peritoneal macrophages (PECs) from both tumor-free (NT-PEC) and AD (AD-PEC) mice (Figure 1E).

To corroborate the evidence that ED stages already promote emergency hematopoiesis, we performed histopathological and immunohistochemical analysis of both spleens and BM from mice bearing early- and late-stage tumor (Figure 2A). Histopathological analysis of the BM parenchyma of wild-type (WT) and *Rorc1*$^{-/-}$ tumor-free and tumor-bearing mice (including ED and AD tumor stages) showed a significant expansion of the granulocytic compartment (Figure 2A, top), which associated with a progressive contraction of the erythroid colonies (blue arrows) and with signs of dysmegakaryopoiesis (i.e., megakaryocytes with bulbous and/or hypolobated nuclei and prominent pleiomorphism; red arrows). Notably, at late time points (AD), the BM granulocytic hyperplasia of tumor-associated emergency hematopoiesis was characterized by the enrichment in immature myeloid precursors (Figure 2A, top, dashed lines), which were more conspicuous in WT than in *Rorc1*$^{-/-}$ mice. As expected, tumor-free mice showed a normal composition of the hematopoietic parenchyma in the BM with preserved myeloid/erythroid ratio and normal maturation of the myeloid elements. Spleen histopathology performed on the same animals demonstrated signs of tumor-associated emergency hematopoiesis in the spleen parenchyma of ED and AD tumor-bearing WT and *Rorc1*$^{-/-}$ mice, in the form of red pulp hyperplasia underlying splenomegaly (Figure 2A, bottom). The enhanced myelopoiesis of WT mice featured the progressive (i.e., from ED to AD) accumulation of clusters of morphologically immature granulocytes (Figure 2A, bottom, arrows and dashed lines; right H&E insets) that intermingled with erythroid precursor islets, megakaryocytes, and polymorphonuclear granulocytes. Despite a comparable degree of red pulp hyperplasia due to the consistent increase in polymorphonuclear granulocytes, erythroid precursors, and megakaryocyte clusters, *Rorc1*$^{-/-}$ mice showed less clusters of morphologically immature myeloid cells as compared with their WT counterparts (Figure 2A, bottom, arrows and dashed lines; right H&E insets). Immunohistochemical analysis of the MDSC-associated IL-4R marker highlighted IL-4R$^+$ myeloid cells with monocytoid or granulocytic morphology populating the myeloid cell aggregates differently enriched within the expanded red

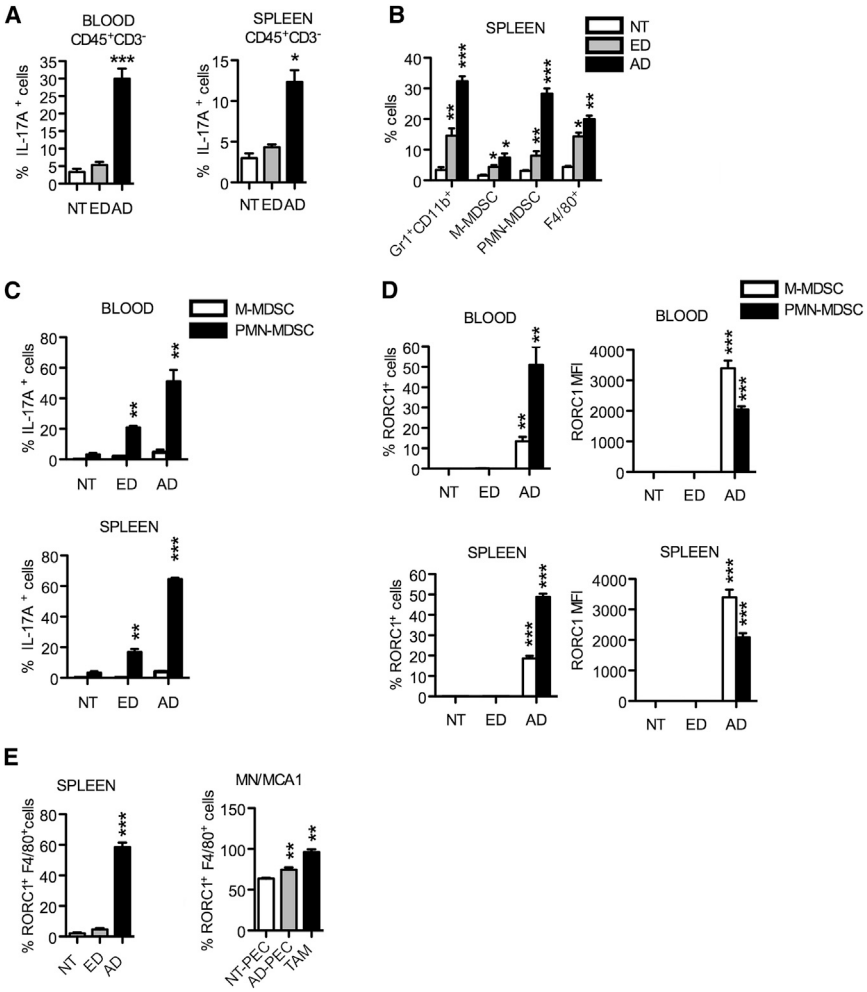

Figure 1. Myeloid-Specific IL-17A$^+$/RORC1$^+$ Cells Mark Advanced Cancer-Associated Inflammation

(A) Expression of IL-17A by CD45$^+$CD3$^-$ hematopoietic cells in blood (left) or spleens (right) from tumor-free (NT) or MN/MCA1-bearing mice, at both early tumor disease (ED) and advanced tumor disease (AD). Mean percentages ± SEM of IL-17A$^+$ cells within the CD45$^+$CD4$^-$CD3$^-$ gate were measured by fluorescence-activated cell sorting (FACS).

(B) Myeloid subsets in spleens from tumor-bearing mice. Mean percentages ± SEM of Gr1$^+$CD11b$^+$ (total MDSCs), CD11b$^+$Gr1$^+$Ly6C$^+$ Ly6G^{low} (M-MDSCs), CD11b$^+$Gr1$^+$Ly6G$^+$Ly6C^{low} (PMN-MDSCs) and CD11b$^+$F4/80$^+$ cells in spleen from NT, ED, or AD mice measured within the CD45$^+$ gate.

(C) Mean percentages ± SEM of IL-17A-expressing M-MDSCs and PMN-MDSCs in blood or spleens from NT, ED, or AD mice.

(D) Mean percentages and MFI ± SEM of RORC1-expressing M-MDSCs and PMN-MDSCs in blood or spleens from NT or tumor-bearing mice.

(E) RORC1-expressing splenic CD11b$^+$F4/80$^+$ cells obtained from NT, ED, and AD mice (left) or RORC1-expressing PECs obtained from NT (NT-PECs) and AD (AD-PECs) mice and RORC1-expressing TAMs isolated from AD tumors (MN/MCA1) (right). Results are shown as mean percentages ± SEM. Expression of IL-17A and RORC1 in myeloid cells was determined within the CD11b$^+$CD45$^+$ gate. Results of a representative experiment of six independent experiments with six mice/group are shown. Statistical analysis: *$p < 0.05$, **$p < 0.01$, ***$p < 0.001$ (Student's t test).

See also Figure S1.

pulp of tumor-bearing WT and *Rorc1*$^{-/-}$ mice (Figure 2A). Overall, these results demonstrate that *Rorc1*$^{-/-}$ mice effectively instruct BM and splenic emergency hematopoiesis along cancer development while displaying a defective induction of specific MDSC-related myeloid populations.

With the gating strategy used to determine IL-17A and RORC1 shown in Figure 2B, our results suggest that RORC1 expression is uncoupled from IL-17A in the monocytic/macrophage compartment, while it is co-expressed in the granulocytic cells of tumor-bearing mice. To validate this finding in cancer patients, we analyzed the MDSC populations in PBMCs from healthy donors (HDs; n = 10) or patients with advanced colorectal cancer (CRC; stage II/III; n = 10) using the gating strategy of Figure 2C. It is noteworthy that the number of RORC1$^+$ M-MDSCs (HLA-DR$^{low/-}$CD14$^+$CD33^{high}) and PMN-MDSCs (HLA-DR$^{low/-}$CD15$^+$ CD33^{high}) increased in CRC patients and dominated in the human PMN-MDSC subset (Figure 2D). Expansion of MDSC populations in cancer patients was paralleled by an increased number of circulating neutrophils and monocytes (Figure 2D). Also in analogy to the murine setting (Figure 1D), the human M-MDSC population showed higher mean fluorescence intensity of RORC1$^+$. In contrast, IL-17A was detected neither in human blood M-MDSCs nor in PMN-MDSCs (data not shown). These results indicate that expression of RORC1 by myeloid subsets constitutes a hallmark of tumor-promoting "emergency" myelopoiesis.

RORC1 Promotes Expansion of MDSCs and TAMs

To investigate the in vivo relevance of RORC1-expressing myeloid cells, we transplanted donor RORC1-deficient BM cells into lethally irradiated C57BL/6 WT recipient mice (*Rorc1*$^{-/-}$>WT), to be compared to WT>WT mice. Eight weeks later, mice were injected with MN/MCA1 cells and monitored for tumor development. Tumor growth and metastasis were significantly reduced in *Rorc1*$^{-/-}$>WT mice (Figure 3A). The effect of RORC1 deficiency in BM cells was tested in two additional tumor models. *Rorc1*$^{-/-}$ BM was transplanted into mouse mammary tumor virus-polyoma middle T antigen (MMTV-PyMT; a spontaneous mammary carcinoma [Guy et al., 1992]) transgenic mice and into C57BL/6 mice that were exposed to methylcholanthrene-induced cancerogenesis and subsequently developed fibrosarcoma (Stutman, 1974) (Figure 3B). Consistently, RORC1 deficiency in the BM resulted in tumor growth inhibition in both models (Figure 3B). FACS analysis (data not shown) confirmed the IL-17/RORC1 expression pattern observed in the MN/MCA1 model (Figure 1). *Rorc1*$^{-/-}$>WT

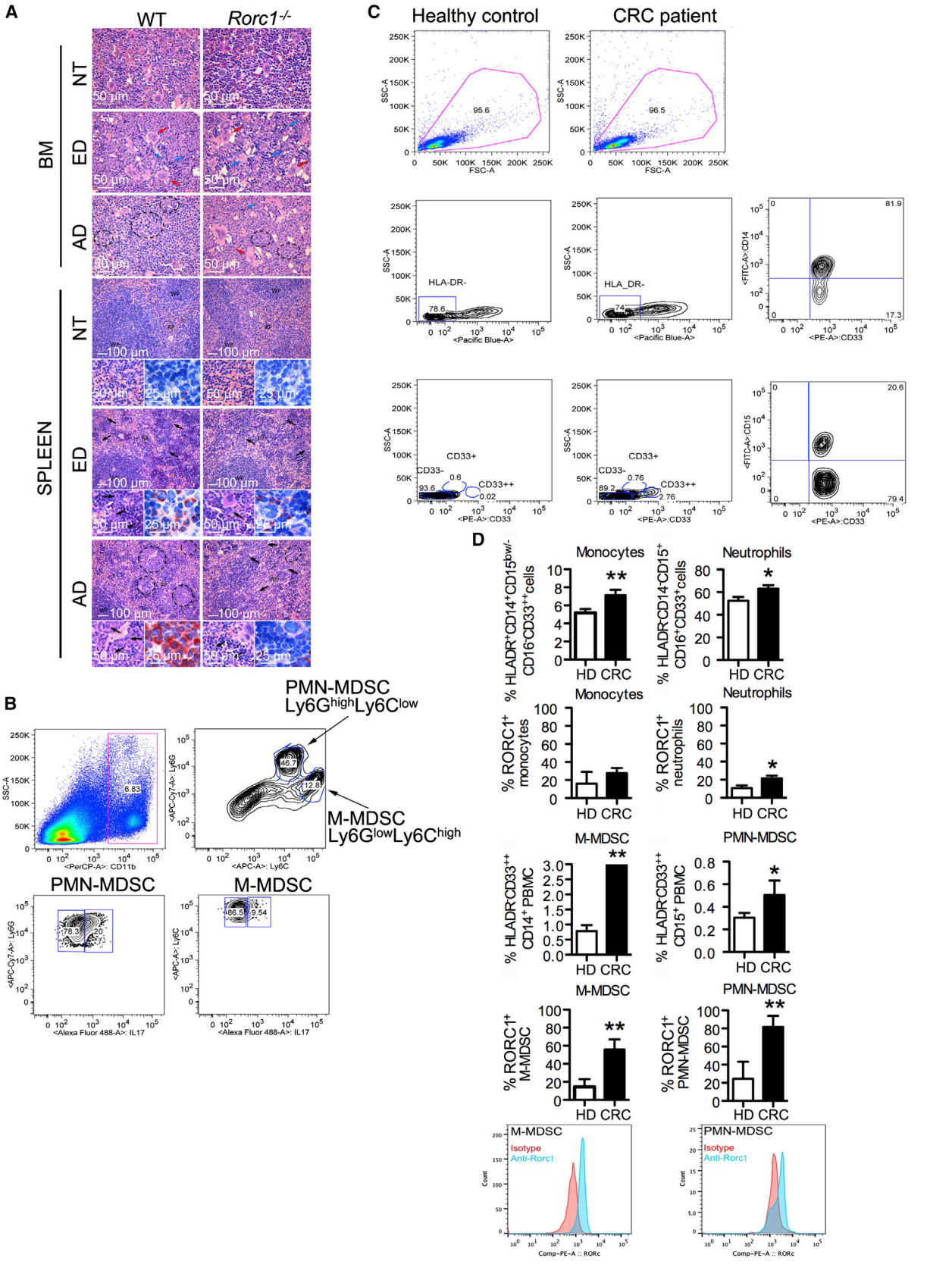

(legend on next page)

tumor-bearing mice showed a significant reduction of splenic M-MDSCs and PMN-MDSCs, in comparison to WT>WT mice (Figure 3C). To estimate the suppressive activity of M-MDSCs, we activated cells with IFN-γ (Gabrilovich et al., 2012), loaded them with ovalbumin, and then co-cultured them for 3 days with total splenocytes purified from OT-1 transgenic mice expressing the T cell receptor specific for the ovalbumin antigen. *Rorc1*$^{-/-}$ M-MDSCs displayed reduced suppressive activity, estimated as proliferation of co-cultured OT1 splenocytes (Figure 3D). It is noteworthy that, at the tumor site, we observed an increase of PMN-MDSCs (Figure 3E), as opposed to a significant decrease of CD11b^{+}Ly6C^{low}F4/80^{+} TAMs (Figure 3F). Histological analysis of spleens from *Rorc1*-deficient tumor bearers showed a dramatic reduction in IL-4R^{+} MDSCs (Marigo et al., 2010) and strongly reduced expression of IL-17A (Figure 3G) in comparison to WT counterpart. These results are further confirmative of the IL-4R expression analyses on WT and *Rorc1*$^{-/-}$ BM (Figure 2A) and imply that RORC1 promotes the expansion of splenic MDSCs and TAMs. To confirm this conclusion, we treated tumor-free or MN/MCA1-bearing WT mice with the RORC1 agonist SR1078 (Kojetin and Burris, 2014). SR1078 increased the AD lung metastatic burden (Figure S2A), as well as splenic M-MDSCs and PMN-MDSCs (Figure S2B, left). Despite the fact that CD11b^{+}F4/80^{+} macrophages were not modified (data not shown), SR1078 increased RORC1 expression in splenic macrophages, as well as in M-MDSCs and PMN-MDSCs (Figure S2B). By contrast, IL-17A expression was selectively induced in PMN-MDSCs (Figure S2B, right). Of note, SR1078 did not affect steady-state myelopoiesis in tumor-free mice (Figure S2C), confirming RORC1 as a positive regulator of myelopoiesis in cancer.

To explain the reduction of MDSCs in *Rorc1*$^{-/-}$ tumor-bearing mice, we considered two possible mechanisms: RORC1 regulates the differentiation of hematopoietic precursors in the BM (Figure 4) and/or RORC1 regulates the survival and maturation of MDSCs (Figure S3). We first analyzed by FACS the commitment of common hematopoietic progenitors in tumor-bearing WT>WT and *Rorc1*$^{-/-}$>WT chimeras. Although in the spleen few Lin^{-}c-kit^{+}Sca-1^{+} (LSK) cells were measured (data not shown), LSK cells were significantly increased in the BM from *Rorc1*$^{-/-}$>WT mice (Figure 4A). Analysis of myeloid progenitors revealed increased number of CMPs in the BM of *Rorc1*$^{-/-}$>WT chimeras and, in accordance, a decrease of granulocyte/macrophage progenitors (GMPs) (Figure 4A). These findings reveal a blockage in differentiation of early hematopoietic progenitors in *Rorc1*$^{-/-}$>WT chimeras and suggest a relevance of RORC1 directly in the BM during the early steps of myeloid cell differentiation. Corroborating this hypothesis, RORC1 was expressed by immature (c-kit^{+}) granulocytes and monocytes in the BM of naive mice (Figure 4B). In the same myeloid cell subsets, IL-17 was found produced mainly by immature neutrophils (Figure 4B). Next, we tested the in situ expression of IL-17A and RORC1 in BM parenchyma of patients undergoing a biopsy for staging of Hodgkin's lymphoma. Consistently, IL-17A staining was localized within myeloid cells with immature morphology, within the precursor-rich areas lining the bone trabeculae (Figure 4C, black arrows). By contrast, mature granulocytes with segmented nuclei barely expressed or did not express IL-17A. Indeed, a neat decreasing gradient was observed in IL-17A expression from para-trabecular areas rich in precursors toward inter-trabecular spaces mainly populated by mature elements (Figure 4C). Notably, double-marker immunohistochemical analysis confirmed that IL-17A^{+} hematopoietic cells did not correspond to Th-17 cells, as they were distinct from the CD3^{+} T elements populating the BM niche (Figure 4D, black arrows). Within the same BM hematopoietic parenchyma, RORC1 (RORγ) expression was detected mostly in myeloid cells with combined cytoplasmatic and nuclear localization (Figure 4E, black arrows). These results in human samples further support that the RORC1/IL-17A program takes part in the regulation of the precursor

Figure 2. Effects of RORC1 on Emergency Hematopoiesis Associated with Cancer Development

(A). Top: BM histopathological analysis of WT (left) and *Rorc1*$^{-/-}$ (right) tumor-free (NT) and tumor-bearing mice with early (ED) and advanced (AD) disease, showing the progressive changes in BM hematopoietic parenchyma along tumor development in the two strains. While tumor-free mice displayed a normal hematopoietic composition with no detectable differences between WT and *Rorc1*$^{-/-}$ strains, ED and AD BM samples showed a progressive expansion of the myeloid granulocytic lineage, which was paralleled by the contraction of the erythroid (blue arrows) and megakaryocytic (red arrows) compartments and was similarly observed in WT and *Rorc1*$^{-/-}$ mice. In AD samples, the myeloid pool expansion was also characterized by the increase in morphologically immature myeloid cell clusters (dashed lines), which was consistent with the enhanced myelopoietic activitiy of stress-adapted (i.e., cancer-associated) myelopoiesis. The immature myeloid cell clusters characterizing AD samples were more prominent in WT than in *Rorc1*$^{-/-}$ mice. Original magnifications of H&E panels are ×400. Bottom: spleen histopathological analysis of WT (left) and *Rorc1*$^{-/-}$ (right, composite panels) tumor-free (upper panels) and tumor-bearing (ED, middle composite panels; AD, lower composite panels) mice showing the progressive increase in red pulp (RP) hematopoietic function along tumor development in the two strains. In tumor-free mice, white pulp (WP) areas are predominant over RP, the latter being mainly populated by erythroid cells with scattered myeloid and megakaryocytic elements (upper H&E panels and upper H&E insets). In ED and AD samples, RP hyperplasia was evident and consequent to the increase of hematopoietic foci. In particular, the RP WT mice showed an increase in immature myeloid cell figures (left middle and lower H&E panels, arrows and dashed lines) showing granulocytic or monocytoid morphology (left middle and lower H&E insets, arrows), along with an increase in megakaryocyte and erythroid precursor clusters. In *Rorc1*$^{-/-}$ mice, despite a comparable degree of RP hyperplasia mainly consequent to megakaryocyte and polymorphonuclear granulocyte expansion and clustering, foci of morphologically immature myeloid cells were less evident (right middle and lower H&E panels and insets, arrows and dashed lines). Within the RP myeloid cell clusters that were differently expanded in WT and *Rorc1*$^{-/-}$ mice, cells with granulocytic or monocytoid morphology expressing the MDSC marker IL-4R were detected (IHC insets, red signal).

(B) Gating strategy used to determine the different mouse myeloid subsets.

(C) Gating strategy used to determine the different human myeloid subsets.

(D) Cytofluorimetric analysis of RORC1 expression in the circulating MDSC subsets, neutrophils, and monocytes from CRC patients as indicated. MDSC analysis was performed on PBMCs, and analysis of neutrophils and monocytes was carried out in whole blood. Mean percentages ± SEM of M-MDSCs (HLA-DR^{-}CD33^{2+}CD14^{+}), PMN-MDSCs (HLA-DR^{-}CD33^{2+}CD15^{+}), monocytes (HLA-DR^{+}CD14^{+}CD15$^{low/-}$CD16^{-}CD33^{2+}), and neutrophils (HLA-DR^{-}CD14^{-}CD15^{+}CD16^{+}CD33^{+}) in blood from healthy donors (HD; n = 10) and CRC patients (n = 10) are shown. Statistical analysis: *p < 0.05, **p < 0.01, ***p < 0.001 (Student's t test). Below, a representative flow-cytometry analysis of RORC1^{+}M-MDSCs and RORC1^{+}PMN-MDSCs from cancer patients is also shown.

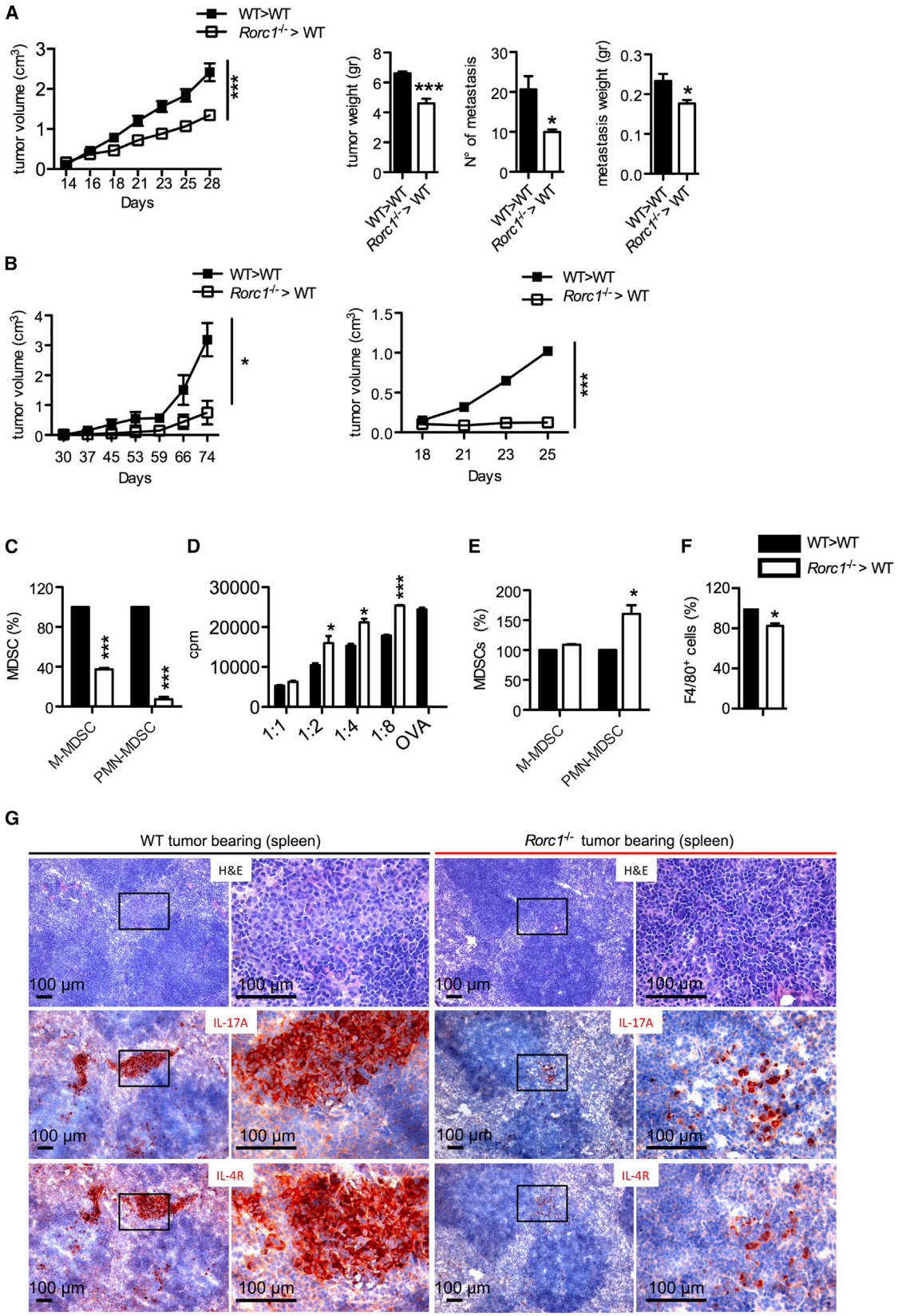

(legend on next page)

compartment during myelopoiesis. To test whether RORC1 regulates myelopoiesis, lineage-negative (Lin^-) cells isolated from WT and *Rorc1*$^{-/-}$ BM were treated in vitro with G-CSF or GM-CSF and tested, 5 days later, for granulocyte or monocyte differentiation by flow cytometry (Figure 4F). In response to GM-CSF, Lin^- cells from *Rorc1*$^{-/-}$ mice failed to differentiate in macrophages, displaying increased differentiation into GR-1^{high} granulocytes. On the contrary, G-CSF treatment resulted in reduced GR-1^{high} granulocyte production by RORC1$^{-/-}$ Lin^- cells. This contrasts with the steady-state condition, where in absence of any specific stimulus the rate of differentiation of Lin^- cells was identical between WT and *Rorc1*$^{-/-}$ BM sources. These results indicated a key role of RORC1 in the myelopoietic activity of G-CSF and GM-CSF. Figure S3A underlies the different effects of G-CSF and GM-CSF on the differentiation of $Ly6G^+$ subsets, indicating that GM-CSF promotes a larger expansion of double $Ly6G^+Ly6C^+$ monocytic cells.

We next determined whether RORC1 might control MDSC survival (Sinha et al., 2011) and maturation. Small differences were observed in survival of WT versus *Rorc1*$^{-/-}$ BM-derived MDSCs at steady-state conditions (medium) (Figure S3B). In contrast, increased $AnxV^+$ binding was observed in both M-MDSCs and PMN-MDSCs after 48 hr, which was reduced in the presence of either tumor supernatant (TSN) or combination of GM-CSF/G-CSF in both subsets (Figure S3B), indicating that RORC1 is crucial for MDSC survival. The protective role of both TSN and GM-CSF/G-CSF against apoptosis was partially lost in RORC1-deficient M-MDSCs, while RORC1-deficient PMN-MDSCs suffered a massive apoptosis (Figure S3B). These results confirm the protective role of RORC1 in CSF-mediated M-MSDC and PMN-MDSC survival, highlighting a tighter dependence of PMN-MDSC survival from RORC1 expression levels.

Neutrophil activation and maturation is paralleled by upregulation of the FCγII and FCγIII receptors (CD32 and CD16, respectively) (Hogarth, 2002) and of the complement C5a receptor (C5aR) (Guo and Ward, 2005). Splenic PMN-MDSCs from WT>WT tumor bearers expressed lower CD16/CD32 and C5aR levels than did PMN-MDSCs from *Rorc1*$^{-/-}$>WT mice (Figure S3C). Furthermore, WT splenic immature PMN-MDSCs expressed lower levels of CD16/CD32 and C5aR, as opposed to higher RORC1, when compared to mature thioglycollate-elicited neutrophils (Neu-PECs) (Figure S3D). These observations indicate that RORC1 might suppress neutrophil maturation, favoring immature PMN-MDSCs to support tumor promotion.

RORC1 Controls Critical Regulators of Myelopoiesis

To determine the tumor-derived factor/s that activate RORC1, we analyzed MN/MCA1 supernatants from AD mice for myeloid growth factors. TSNs were enriched in G-CSF, GM-CSF, and M-CSF and partially in IL-1β (Figure 5A). Of note, 48 hr of treatment with either a combination of GM-CSF and G-CSF or TSN induced IL-17A expression in BM-derived PMN-MDSCs and, to a lower extent, in M-MDSCs (Figure 5B, left). BM-derived M-MDSCs and PMN-MDSCs expressed basal RORC1 levels (Figure 5B, right), plausibly induced by GM-CSF and G-CSF used for their in vitro generation (Peranzoni et al., 2010), which was increased by combination of GM-CSF and G-CSF (Figure 5B, right). Confocal microscopy demonstrated that RORC1 expression and nuclear translocation was induced in naive PECs challenged for 72 hr with lipopolysaccharide (LPS), IL-1β, G-CSF, GM-CSF, and M-CSF, but not by IFN-γ (Figure 5C) or IL-6 (data not shown). Of note, we found increased levels of G-CSF and GM-CSF in the sera of AD mice (data not shown), as compared to ED mice, suggesting that RORC1-dependent emergency hematopoiesis is controlled by the extent of cancer-associated inflammation.

Finally, we determined the mRNA levels for RORC1 and RORC2 (Ivanov et al., 2006; Yang et al., 2008) in PECs and in thymocytes (Sun et al., 2000) from healthy WT mice (Figure S4A). It is noteworthy that LPS-stimulated (72 hr) PECs expressed *Rorc1* mRNA levels similar to those of WT thymocytes, but not *Rorc2* mRNA. These data confirm that in cancer, the monocyte-macrophage lineage expresses a selective RORC1 fingerprint unlinked from IL-17A, whereas the granulocyte/neutrophil lineage expresses a dual RORC1/IL-17A signature. In support of RORC1 as a key driver of "emergency" granulo-monocytopoiesis, BM-$CD11b^+Gr1^+$ granulocytes and BM-$CD11b^+Ly6C^+$ monocytes from both LPS- and M-CSF-treated mice significantly increased RORC1 expression (Figure S4B).

To determine the in vivo role of myeloid growth factor/s, we treated MN/MCA1-bearing mice with neutralizing antibodies to G-CSF, GM-CSF, or the M-CSF receptor (M-CSFR/CSFR1)

Figure 3. Role of RORC1 in the Expansion of MDSCs and TAMs during Tumor-Driven Emergency Myelopoiesis

(A) MN/MCA1 cells were injected into the indicated hematopoietic reconstituted mice. Starting from day 14 after MN/MCA1 cell injection, tumor volume (cm^3) was monitored. At day 28, mice were sacrificed, the weight of the tumors (g) was estimated (left), and the number and weight of macroscopic lung metastases was measured (right). Data are shown are the mean ± SEM of at least 12 mice/group. Statistical analysis: *p < 0.05, **p < 0.01, ***p < 0.001 (Student's t test).

(B) *Rorc1*$^{-/-}$ BM was transplanted into MMTV-PyMT transgenic mice (left) or C57Bl/6 mice, which were subsequently exposed to methylcholanthrene to induce fibrosarcoma (right). Mean tumor volumes (cm^3) ± SEM from six WT>WT and *Rorc1*$^{-/-}$>WT chimeras are shown. Statistical analysis: *p < 0.05, **p < 0.01, ***p < 0.001 (Student's t test).

(C) Mean percentages ± SEM of M-MDSCs and PMN-MDSCs in spleens from WT>WT and *Rorc1*$^{-/-}$>WT tumor (MN/MCA1) bearers. Statistical analysis: *p < 0.05, **p < 0.01, ***p < 0.001 (Student's t test).

(D) Decreased antigen-specific (OVA) suppressive activity of *Rorc1*$^{-/-}$ M-MDSCs in response to IFN-γ at different MDSC:OT1 splenocyte ratios. Data shown are the mean ± SEM of a representative experiment done in triplicate. Statistical analysis: *p < 0.05, **p < 0.01, ***p < 0.001 (Student's t test).

(E) Mean percentages ± SEM of M-MDSCs and PMN-MDSCs in primary AD tumors (MN/MCA1) from WT>WT and *Rorc1*$^{-/-}$>WT mice (AD). Statistical analysis: *p < 0.05, **p < 0.01, ***p < 0.001 (Student's t test).

(F) Mean percentages ± SEM of $F4/80^+$ TAMs in primary tumors from WT>WT and *Rorc1*$^{-/-}$>WT tumor bearers (MN/MCA1). Myeloid cell percentage in *Rorc1*$^{-/-}$>WT chimeras (white bar) is represented as relative value as compared to WT>WT chimeras (100%) (black bar). Data from a representative experiment, of six independent experiments, with n = 6 mice per group is shown. Statistical analysis: *p < 0.05, **p < 0.01, ***p < 0.001 (Student's t test).

(G) Histological analysis of $IL\text{-}17A^+$ and $IL\text{-}4R^+$ in the splenic MDSC population in WT and *Rorc1*$^{-/-}$ tumor-bearing mice.

See also Figure S2.

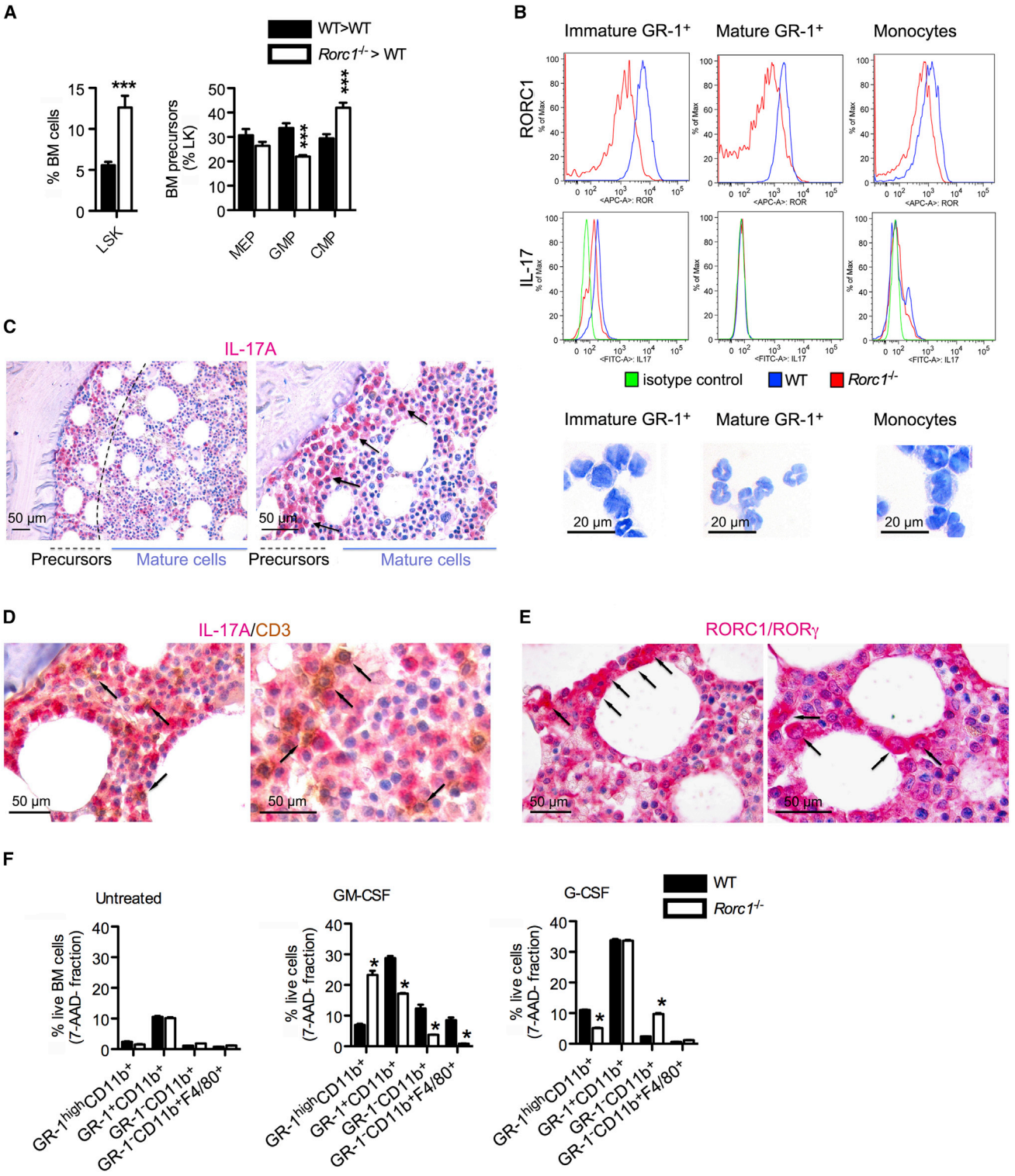

Figure 4. RORC1 Regulates Myeloid Commitment of BM Precursors

(A) Frequency of hematopoietic stem cells (LSK) and myeloid progenitors (CMP, GMP, and MEP) in the BM of WT and *Rorc1*$^{-/-}$ mice. Mean percentages ± SEM is shown. Statistical analysis: *p < 0.05, **p < 0.01, ***p < 0.001 n = 6 (Student's t test).

(B) Flow-cytometry analysis for the expression of RORC1 and IL-17 in different myeloid cells identified by staining of BM cells with monoclonal antibodies to CD11b, CD117, GR-1, and F4/80. For RORC1 expression, BM cells from *Rorc1*$^{-/-}$ mice were set as a negative control. Immature granulocytes (myeloblasts) were identified according to their co-expression of GR-1 and c-kit. Mature granulocytes were GR-1^{high} and c-kit^{-}, whereas monocytes/macrophages were CD11b^{+}Gr-1^{-}F4/80^{+}. For further checking of their phenotype, these populations were sorted and stained with Giemsa. Representative pictures are shown.

(legend continued on next page)

(Hume and MacDonald, 2012). Inhibition of G-CSF and GM-CSF limited the accumulation of splenic PMN-MDSCs with no effect on M-MDSCs (Figure 5D, left). In contrast, the anti-CSFR1 antibody decreased the number of F4/80$^+$ spleen macrophages whereas, surprisingly, it induced a strong increase in splenic PMN-MDSCs. At contrast, the anti-G-CSF antibody significantly increased the CD11b$^+$F4/80$^+$ spleen macrophages. Confirming the relevance of myelopoiesis to cancer inflammation, neutralization of GM-CSF, G-CSF, or M-CSFR resulted in inhibition of tumor growth and metastasis (Figure 5D, center and right). These findings suggest a reciprocal antagonistic regulation of the polymorphonuclear and monocytic lineages in CSF-driven "emergency" myelopoiesis in cancer.

To shed light on the mechanisms of RORC1-driven emergency myelopoiesis, we evaluated positive and negative transcriptional regulators in BM and spleens from WT>WT and *Rorc1*$^{-/-}$>WT tumor bearers. CCAAT/enhancer binding protein β (C/EBPβ) is a major positive regulator of G-CSF- and GM-CSF-driven "emergency" myelopoiesis (Akagi et al., 2008), whereas C/EBPα appears to be a major regulator of "steady-state" granulopoiesis and cooperates with PU.1 to "emergency" granulo-monocytopoiesis (Hirai et al., 2006; Jin et al., 2011). We observed a mild but significant decrease of mRNA expression of PU.1, C/EBPβ, and C/EBPα in spleens and BM from *Rorc1*$^{-/-}$>WT tumor bearers, paralleled by decreased C/EBPβ protein levels in splenic PMN-MDSCs and M-MDSCs (Figure 6A). Importantly, BM and spleens from *Rorc1*$^{-/-}$>WT MN/MCA1 tumor bearers displayed increased mRNA levels of the suppressor of cytokine signaling-3 (Socs3) and the transcriptional co-regulator B cell leukemia/lymphoma 3 (Bcl3) (Figure 6B), both potent inhibitors of G-CSF-driven granulopoiesis (Croker et al., 2004; Kreisel et al., 2011). In agreement with the IFN-γ-mediated inhibition of G-CSF-driven neutrophilia (Ulich et al., 1988), IFN-γ induced a strong increase of Socs3 and Bcl3 mRNA in splenic PMN-MDSCs from *Rorc1*$^{-/-}$ tumor bearers (Figure 6B, right). Finally, in accordance with the decreased number of macrophages found in spleen and tumor of *Rorc1*$^{-/-}$>WT chimeras (Figure 6C), we observed a decreased number of IRF8-expressing CD11b$^+$F4/80$^+$CD115$^+$ macrophages (Figure 6D), which was confirmed by confocal microscopy in tumor tissues of *Rorc1*$^{-/-}$>WT chimeras (data not shown). As M-CSFR/CD115 (Qian and Pollard, 2010) is a marker of terminally differentiated macrophages (Auffray et al., 2009), this result indicates that RORC1 is required for the modulation of cell-fate switching factor(s) driving maturation of macrophages (Friedman, 2007).

RORC1 Controls Polarization of Myeloid Cells

M-CSFR signaling modulates macrophage survival and differentiation (Qian and Pollard, 2010) and induces M2 macrophage polarization, a condition supporting tumor progression (Mantovani and Sica, 2010). To evaluate RORC1 in the macrophage polarization, we analyzed the mRNA expression of prototypical M1 and M2 genes in AD-PECs, cells displaying an intermediate PEC versus a TAM phenotype and representing a good model to study M1-M2 polarization in cancer (Sica et al., 2000; Torroella-Kouri et al., 2009) from tumor-bearing WT>WT and *Rorc1*$^{-/-}$>WT chimeras. AD-PECs were isolated from tumor-bearing WT>WT and *Rorc1*$^{-/-}$>WT chimeras and treated with 100 ng LPS (M/L) or 200 U/ml IFN-γ for 4 hr to induce M1 polarization or exposed to LPS for 20 hr (L/M) to induce LPS-tolerant M2-like polarization (Porta et al., 2009). In addition, spleen PMN-MDSCs were stimulated 4 hr in vitro with IFN-γ, LPS, or IFN-γ plus LPS. RORC1-deficient AD-PECs displayed enhanced expression of M1 (IL-12p40, tumor necrosis factor alpha [TNF-α], IL-1β) and decreased expression of M2 (IL-10, TGFβ, chitinase-3-like protein 3/Ym1) genes under M/L and L/M conditions (Figure 7A). Simiarly, RORC1-deficient PMN-MDSCs showed increased TNF-α and IL-1β mRNA levels and IL-1β secretion in response to LPS/IFN-γ (Figure 7B). Thus, RORC1 acts as negative regulator of M1 and promoter of M2 cytokine genes. This observation was supported by the increased levels of pro-inflammatory cytokines (TNF-α and IL-1β) and growth factors (G-CSF, GM-CSF, and VEGF) in MN/MCA1 supernatants from *Rorc1*$^{-/-}$>WT (Figure 7C), correlating with marked splenomegalia observed in *Rorc1*$^{-/-}$>WT chimeras bearing the MN/MCA1 and MMTV-PyMT tumors (Figure 7D). Moreover, we found increased splenic CD4$^+$IFN-γ$^+$ and F4/80$^+$TNF-α$^+$ cells in tumor-free and tumor-bearing *Rorc1*$^{-/-}$>WT mice (Figure S5A), while total CD45$^+$CD4$^+$ cells decreased as described (Figure S5A) (Harrington et al., 2005). In contrast, tumor-infiltrating CD4$^+$IFN-γ$^+$ and total CD45$^+$CD4$^+$ T cells increased in *Rorc1*$^{-/-}$>WT chimeras (Figure S5A). Furthermore, F4/80$^+$TNF-α$^+$ macrophages increased in spleens and tumors from *Rorc1*$^{-/-}$>WT mice (Figure S5A). Supporting the inhibitory role of RORC1, CD4$^+$Foxp3$^+$ T regulatory cells significantly decreased in the spleen from *Rorc1*$^{-/-}$>WT mice (Figure S5A).

Antagonistic Regulation of the Polymorphonuclear and Monocytic Lineages

A decreased number of tissue macrophages in tumors from *Rorc1*$^{-/-}$>WT mice (Figure 3F) correlated with increased PMN-MDSC infiltration (Figure 3E), suggesting that pathways leading to terminal differentiation and M2 polarization of TAMs hamper neutrophil accumulation in tumors. To prove this assumption, we treated MN/MCA1-bearing WT mice with an anti-CSFR1 antibody (Ries et al., 2014), which significantly depleted the CD11b$^+$F4/80$^+$CD115$^+$ TAM population, co-expressing high RORC1 levels (Figure 8A). Macrophage depletion was paralleled by the inhibition of immature RORC1$^+$ M-MDSCs and PMN-MDSCs (Figure 8B) and increased tumor infiltration of mature (C5a^{high}CD16/32^{high}) (Figure 8C) RORC1$^-$Ly6G^{high} neutrophils (Figure 8B). In agreement, RORC1 was highly expressed in

(C–E) In situ expression of IL-17A and RORC1 (RORγ) within the hematopoietic BM parenchyma of patients undergoing BM biopsy for staging of Hodgkin's lymphoma (HL). Representative pictures show that both IL-17A (C) and RORC1 (E) are produced by immature BM cells lining the endosteal niche, whereas IL-17A is not expressed by CD3$^+$ cells in the BM (D).

(F) Lin$^-$ cells were isolated from the BM of WT and *Rorc1*$^{-/-}$ mice and treated as indicated. The frequency of differentiated myeloid cell subsets was calculated within the gate of viable cells (7-AAD-). Data shown are the mean ± SEM of two different experiments. Statistical analysis: *p < 0.05, **p < 0.01, ***p < 0.001 (Student's t test).

See also Figure S3.

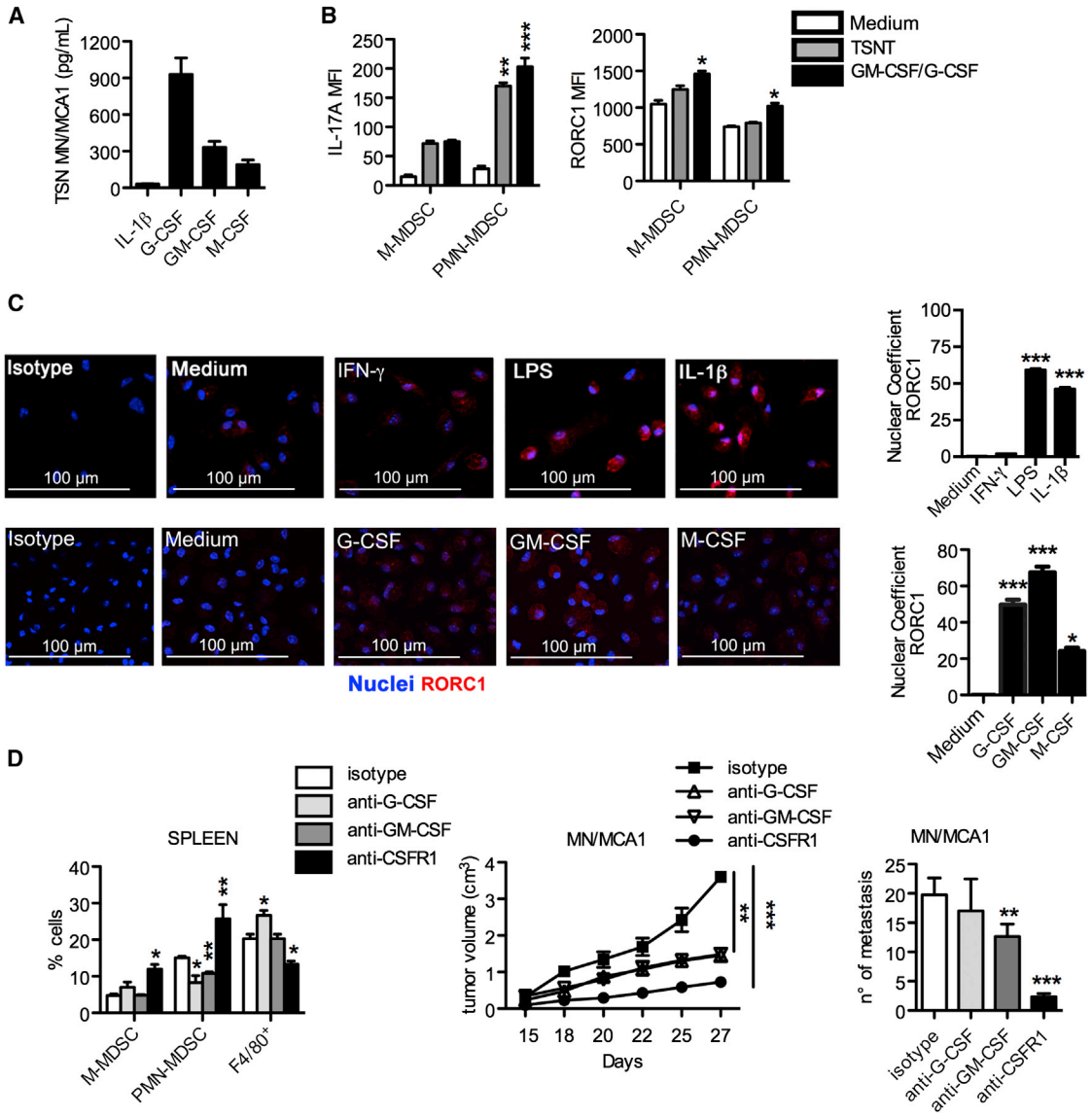

Figure 5. CSF-, LPS-, and IL-1β-Mediated Induction of RORC1 in Innate Immune Cells

(A) Expression levels of GM-CSF, G-CSF, M-CSF, and IL-1β in the MN/MCA1 supernatants (TSN) from advanced disease were determined by ELISA. Data shown are the mean ± SEM of three independent experiments.

(B) BM-MDSCs were left untreated or were treated with either TSN (MN/MCA1) or a combination of recombinant GM-CSF (40 ng/ml) and G-CSF (40 ng/ml) for 48 hr. Expression of IL-17A and RORC1 in M-MDSCs and PMN-MDSCs was evaluated by FACS analysis. Mean fluorescence intensity (MFI) ± SEM of three representative experiments is shown. Statistical analysis: *$p < 0.05$, **$p < 0.01$, ***$p < 0.001$ (Student's t test).

(C) Expression and nuclear translocation of RORC1 in PECs exposed to IFN-γ (200 U/ml), LPS (100 ng/ml), IL-1β (20 ng/ml), G-CSF (40 ng/ml), GM-CSF (40 ng/ml), and M-CSF (40 ng/ml). After 72 hr of in vitro activation, PECs were stained with anti-RORC1 antibody (red) or irrelevant rat immunoglobulin G (IgG). Nuclei were counterstained with DAPI (blue). Representative images are shown. Confocal microscopy analysis of RORC1 nuclear fluorescence intensity (nuclear coefficient) is shown on the right. Mean ± SEM from three independent experiments is shown. Statistical analysis: *$p < 0.05$, **$p < 0.01$, ***$p < 0.001$ (Student's t test).

(D) MN/MCA1 tumor-bearing mice were treated with blocking antibodies against G-CSF, GM-CSF, M-CSFR/CSFR1, or isotype control antibody as indicated. Data on M-MDSCs, PMN-MDSCs, and $CD11b^+F4/80^+$ cells in spleens from mice with AD within the $CD45^+$ gate (left) and primary tumor growth (center) are shown as the mean ± SEM. The number of macroscopic lung metastases (right) is shown as the mean ± SD. A representative experiment with six mice/ group is shown. Statistical analysis: *$p < 0.05$, **$p < 0.01$, ***$p < 0.001$ (Student's t test).

See also Figure S4.

$F4/80^+/CD115^+$ macrophages, in comparison to reduced RORC1 levels in $Ly6G^{low}$ granulocytes and negativity in mature inflammatory $Ly6G^{high}$ granulocytes (Figure 8D), indicating that TAM infiltration is accompanied by infiltration of immature MDSC populations, at the expense of mature neutrophils. Of relevance, anti-M-CSF treatment resulted in a similar increase of

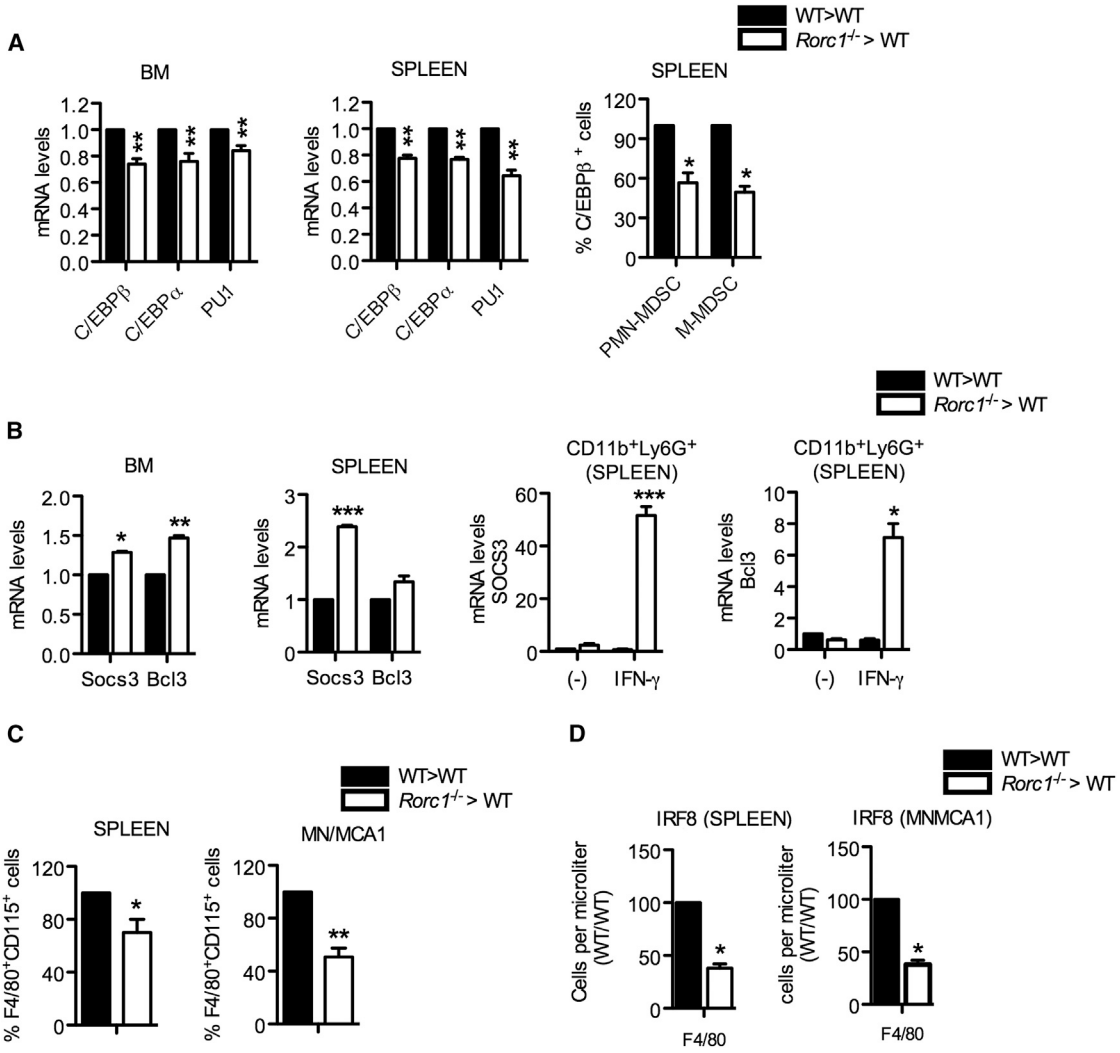

Figure 6. Influence of RORC1 on the Expression of Transcriptional Regulators of Myeloid Cell Maturation

(A) Total RNA from BM (left) and splenocytes (center) obtained from MN/MCA1-bearing WT>WT and *Rorc1*$^{-/-}$>WT mice was analyzed by RT-PCR for the expression of the C/EBPβ, C/EBPα, and PU.1 transcription factors. Results are given as the fold increase over the mRNA level expressed by WT and are representative of at least three different experiments. Mean percentages ± SEM of C/EBPβ protein expression in M- and PMN-MDSC subsets in c-kit^{low} BM and splenocytes from WT>WT and *Rorc1*$^{-/-}$>WT tumor-bearing chimeras were measured by FACS analysis (right). The mean ± SD of three independent experiments is shown.

(B) mRNA levels of Socs3 and Bcl3 in BM and splenocytes (left) or in unstimulated (–) and IFN-γ-activated PMN-MDSCs (CD11b$^+$Ly6G$^+$) isolated from the spleen (right) obtained from MN/MCA1-bearing WT>WT and *Rorc1*$^{-/-}$>WT mice. Results are shown as the mean ± SEM from triplicate values.

(C) Splenic CD11b$^+$F4/80$^+$CD115$^+$ macrophages (left) and CD11b$^+$F4/80$^+$CD115$^+$ TAMs (right). Macrophage percentage in *Rorc1*$^{-/-}$>WT chimeras (white bar) is represented as relative value as compared to WT>WT chimeras (100%) (black bar). Results are shown as the mean ± SEM from triplicate values.

(D) The mean count ± SEM of IRF8$^+$F4/80$^+$ cells in spleens and MN/MCA1 from WT>WT and *Rorc1*$^{-/-}$>WT chimeras analyzed within the CD11b$^+$F4/80$^+$ gate is shown. The mean ± SEM of three independent experiments is shown. Statistical analysis: *p < 0.05, **p < 0.01, ***p < 0.001 (Student's t test).

C5a^{high}CD16/32^{high} mature neutrophils in the spleen (Figure S6A), indicating its systemic effects. These results are in agreement with Figure 5D and together suggest a competition between the monocytic and granulocytic commitment of myeloid precursors.

As mature RORC1$^-$PMN-MDSCs display a pronounced inflammatory phenotype (Figure 7B), their inhibition most likely contributes to maintaining the tumor-promoting microenvironment. Furthermore, while M-CSF induced RORC1 expression in splenic (data not shown) and medullar (Figure S4B) monocyte precursors, treatment with anti-CSFR1 resulted in reduced monocyte/macrophage precursors (population C + D) and in increased granulocyte progenitors (population A + B) (Figure 8E). Supporting the role for reciprocal negative regulation of monocytes/macrophages and granulocytes in cancer inflammation, treatment with anti-G-CSF antibody increased the number of splenic F4/80$^+$TNF-α$^+$ M1-like macrophages, paralleled by elevation of CD4$^+$IFN-γ$^+$ Th1 cells (Figure 8F).

As the increase in CD4$^+$IFN-γ$^+$ and F4/80$^+$TNF-α$^+$ cells observed in *Rorc1*$^{-/-}$ tumor-bearing mice was phenocopied by the anti-G-CSF treatment of MN/MCA1 tumor-bearing

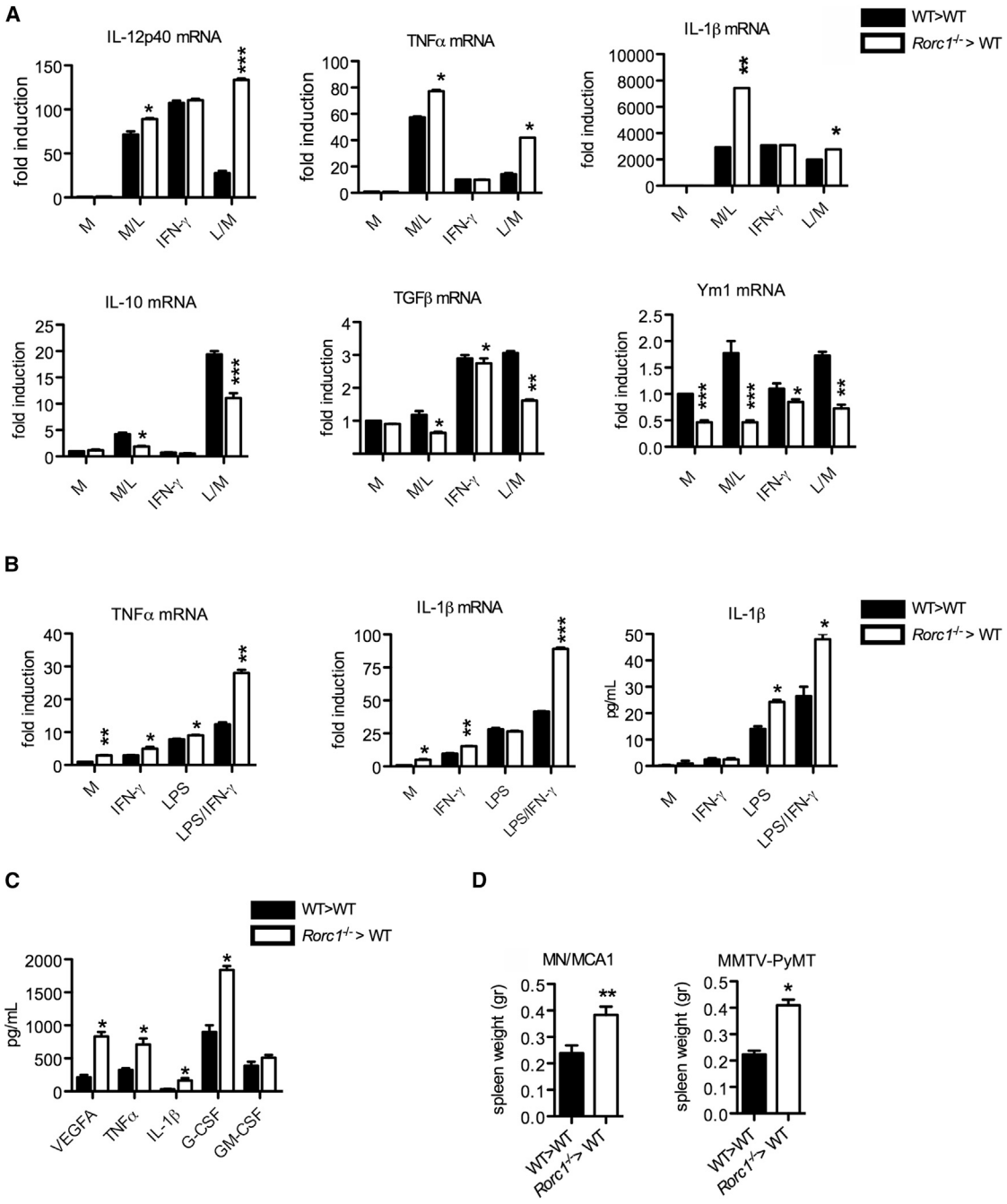

Figure 7. Effects of RORC1 on Macrophage Polarization

(A) Total RNA from control (medium), activated (IFN-γ), M1-activated (M/L), and M2-like LPS-tolerant (L/M) AD-PECs harvested from MN/MCA1 from WT>WT (black bar) or *Rorc1*$^{-/-}$>WT (white bar) chimeras were analyzed by RT-PCR for the expression of representative M1 genes (IL-12p40, TNF-α, and IL-1β) and M2 genes (IL-10, TGFβ, and Ym1). Statistical analysis: *p < 0.05, **p < 0.01, ***p < 0.001; n = 3 (Student's t test). Results are representative of at least three different experiments and are shown as the mean ± SEM from triplicate values.

(B) Total RNA from control (medium) and activated (IFN-γ, LPS, or LPS+IFN-γ) PMN-MDSCs obtained from the spleen from MN/MCA1-bearing WT>WT and *Rorc1*$^{-/-}$>WT chimeras were analyzed by RT-PCR for the expression of representative M1 genes (IL-1β and TNF-α). Secretion of IL-1β (pg/ml) was determined by ELISA. Cells were activated as indicated for 24 hr. Results are given as the fold increase over the mRNA level expressed by untreated cells (medium) and are representative of at least three different experiments; shown are the mean ± SEM from triplicate values. For ELISA, results are the average of three independent experiments ± SD. Statistical analysis: *p < 0.05, **p < 0.01, ***p < 0.001 (Student's t test).

(C) Expression levels (pg/ml) of cytokines/growth factors in tumor supernatants (MN/MCA1) harvested from WT>WT and *Rorc1*$^{-/-}$>WT chimeras. Results are the average of three independent experiments ± SEM. Statistical analysis: *p < 0.05, **p < 0.01, ***p < 0.001 (Student's t test).

(D) Mean spleen weights (g) ± SEM in MN/MCA1-bearing (n = 10) and MMTV-PyMT (n = 6) mice. Statistical analysis: *p < 0.05, **p < 0.01, ***p < 0.001 (Student's t test).

See also Figure S5.

mice, we questioned whether G-CSF might work through RORC. To address this question, we treated WT and *Rorc1*$^{-/-}$ tumor-bearing mice with anti-G-CSF and monitored the expansion of both CD4^{+}IFN-γ^{+} and F4/80^{+}TNF-α^{+} cells. As a result, the anti-G-CSF treatment significantly decreased RORC1 expression in PMN-MDSCs and partially in M- MDSCs and F4/80^{+} macrophages (Figure S6B). Moreover, the increase of tumor-infiltrating F4/80^{+}TNF-α^{+} macrophages and CD4^{+}IFN-γ^{+} T cells in response to anti-G-CSF, observed in WT mice, was significantly reduced in *Rorc1*$^{-/-}$ mice (Figure S6C), strengthening the hypothesis that G-CSF works through the induction of RORC1. Finally, to assess the role of myeloid-specific RORC1 in adaptive immunity against cancer, we depleted CD4^{+} and CD8^{+} T cells in both WT and *Rorc1*$^{-/-}$ tumor-bearing mice. As a result, we observed a significant increase of lung metastasis in *Rorc1*$^{-/-}$ tumor-bearing mice treated with the anti-CD4/anti-CD8 antibodies (Figure S6D), suggesting that the protumor activity of RORC1 acts through both the innate and adaptive immunity.

DISCUSSION

We demonstrate that RORC1 fuels cancer-promoting inflammation by enhancing survival and expansion of CD16/32^{low}/C5aR^{low} immature MDSCs, with reduced expression of M1 cytokines (IL-1β and TNF-α) and increased suppressive activity, and promoting terminal macrophage differentiation. Our study indicates that RORC1 impinges on cancer-driven myelopoiesis by suppressing negative (Socs3 and Bcl3) (Croker et al., 2004; Kreisel et al., 2011) and promoting positive (C/EBPβ) (Hirai et al., 2006) transcriptional regulators of "emergency" granulopoiesis, while instating the expression of macrophage-specific transcription factors IRF8 and PU.1 (Friedman, 2007). Depletion of RORC1^{+}F4/80^{+}CD115^{+} TAMs with anti-CSFR1 antibody enhanced the recruitment of mature (CD16/CD32^{high}) RORC1^{-} inflammatory neutrophils, with diminished expansion of immature RORC1^{+}(CD16^{low}/CD32^{low}) PMN-MDSCs. This result, along with the observed competition between the commitment of myeloid precursors for the monocytic versus granulocytic lineage, observed with the anti-G-CSF and anti-CSFR1 treatments, respectively, may indicate that blocking M-CSF-dependent myelopoiesis unleashes expansion and maturation of granulocytic cells, which would favor the increase of tumor-infiltrating neutrophils. These events deflect the inflammatory microenvironment to adverse the tumor, increasing infiltration of CD4^{+} IFN-γ^{+} T cells and F4/80^{+}TNF-α^{+} M1 polarized macrophages. Our results indicate that high RORC1 expression acts as pro-resolving mediator of myeloid inflammation and that antagonists to RORC1 might hold the potential to prevent tumor-promoting myeloid differentiation. We also report that IL-17 expression is disjointed from RORC1 in the monocyte/macrophage lineage (M-MDSCs and CD11b^{+}F4/80^{+} TAMs). Wu et al. have recently described that tumor-infiltrating inflammatory dendritic cells activate IL-17-producing RORγt^{+} $\gamma\delta$T17 cells to secrete IL-8, TNF-α, and GM-CSF cells and sustain the subsequent intratumor accumulation of immunosuppressive PMN-MDSCs in colorectal cancer (Wu et al., 2014). Further, an inflammatory cascade encompassing the IL-1β-mediated production by IL-17 in $\gamma\delta$T cells resulted in systemic G-CSF-dependent expansion of suppressive neutrophils and formation of breast cancer metastasis (Coffelt et al., 2015). Our observation that IL-17 is selectively expressed, but not secreted by immature granulocyte/neutrophil subsets, does not support a direct role of myeloid-cell-derived IL-17 in the expansion of MDSCs during cancer development, but rather indicates that IL-17A is a hallmark of immature myeloid responses in cancer bearers. This notion is further supported by the observation that expression of IL-17 and RORC1 localizes within the immature myeloid cells precursor-rich areas lining the bone trabeculae of BM biopsies from patients under diagnosis of Hodgkin's lymphoma. Moreover, in contrast to *Rorc1*$^{-/-}$ BM transplantation, chimeric mice receiving the *Il17a*$^{-/-}$ BM had no defect in developing tumor-associated myeloid cells, in both the BM and spleen (data not shown). It remains to be established whether IL-17A expression by circulating MDSCs is dependent on the disease stage, as we did not observe its expression in blood from T2/T3 CRC patients.

Along with other reports, our observation highlights the relevance of members of the nuclear receptor superfamily in regulation of inflammation (Gerbal-Chaloin et al., 2013; Wittke et al., 2004) and suggests RORC1 as central regulator of cancer associated myelopoiesis and key driver of the protumor differentiation of MDSCs and TAMs.

EXPERIMENTAL PROCEDURES

More-detailed procedures can be found in the Supplemental Experimental Procedures.

Ethics Statement

The study was approved by the scientific board of Humanitas Clinical and Research Center and designed in compliance with Italian governing law, EU directives and guidelines, and the NIH Guide for the Care and Use of Laboratory Animals. Mice have been monitored daily and euthanized when displaying excessive discomfort. Cancer patients were enrolled in the study after signing Cancer Research Center Humanitas IRB-approved consent.

Mice

C57BL/6 mice were purchased from Charles River. RORC1 mutant mice (B6.129P2(Cg)-*Rorc*^{tm1Litt}/J) (Sun et al., 2000) were donated by Dr. Dan Littman (New York University). MMTV-PyMT mice (Guy et al., 1992) were donated by Professor Guido Forni (University of Turin) and mated with C57BL/6 females to obtain the F1 C57BL/6-MMTV-PyMT strain. IL-17A-deficient mice were donated by Dr. Burkhard Becher (University of Zurich). All animal work was conducted under the approval of the Humanitas Clinical and Research Center, in accordance with Italian and EU directives and guidelines.

BM Transplantation

5 × 10^{6} CD45.2 RORC1-deficient (*Rorc1*$^{-/-}$), IL-17A$^{-/-}$, or WT BM cells were injected intravenously into 8-week-old lethally irradiated (two doses of 475 cGy) CD45.1 C57BL/6 WT male or C57BL/6-MMTV-PyMT female mice. 8 weeks later, BM engraftment was checked by staining of blood cells with PerCP-conjugated CD45.1 antibody and PE-conjugated CD45.2 antibody (BD Biosciences) and subsequent FACS analysis.

Tumor Models

10^{5} murine fibrosarcoma (MN/MCA1) cells were injected intramuscularly in the left hind limb. Tumor growth was monitored three times a week with a caliper, starting from day 14. The models of chemically induce fibrosarcoma and mammary tumor virus-polyoma middle T antigen (MMTV-PyMT) transgenic mice are described in the Supplemental Experimental Procedures.

Cell Culture and Reagents

Lineage cell separation from BM, isolation of myeloid cells, and cell-culture conditions are described in the Supplemental Experimental Procedures.

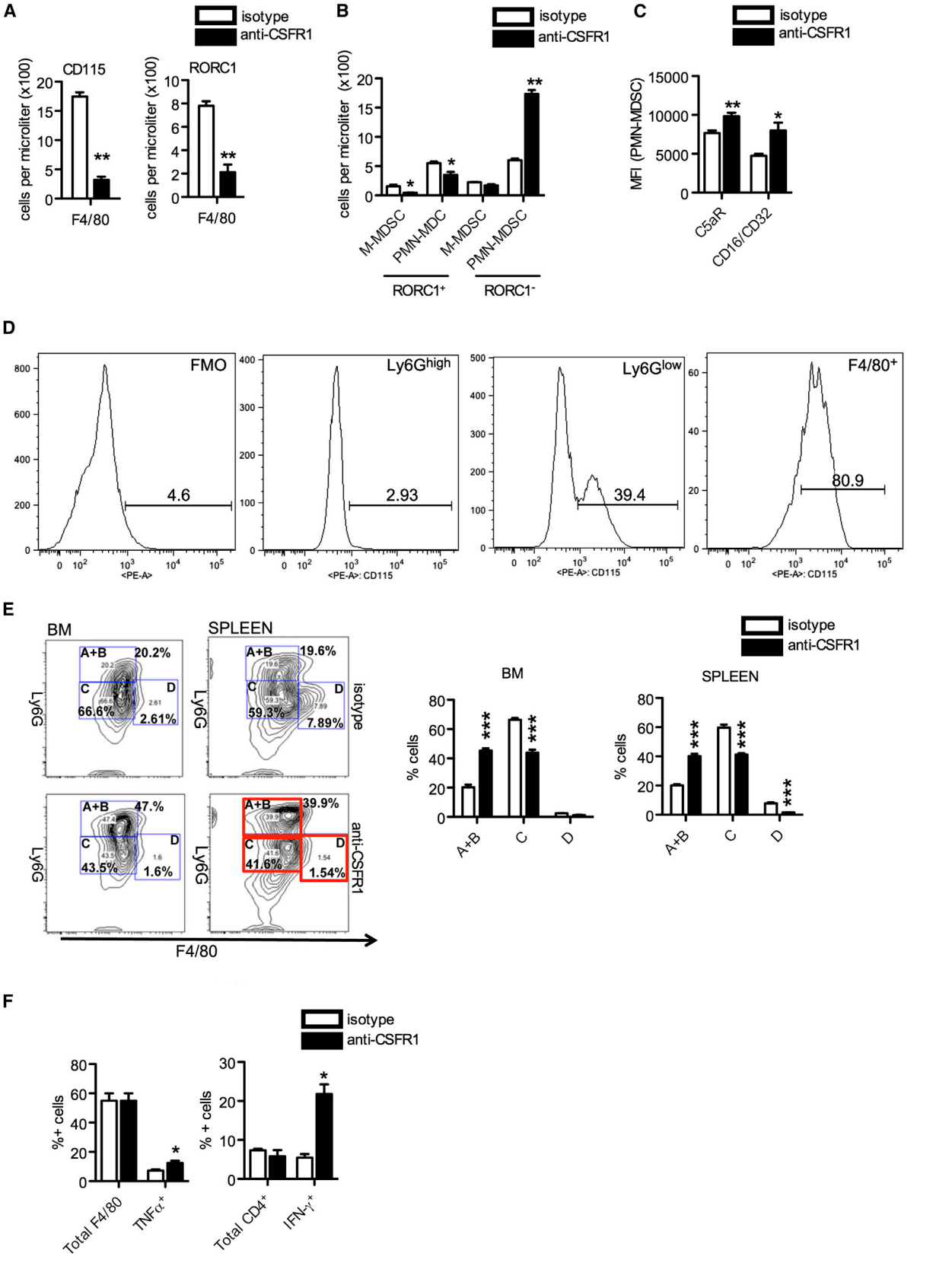

(legend on next page)

Mixed-Lymphocyte Reaction

Mixed-lymphocyte reaction was performed as previously reported (Larghi et al., 2012) and as described in the Supplemental Experimental Procedures.

Patients

Ten patients with T2 or T3 CRC did not receive radiation or chemotherapy before sample collection.

Flow Cytometry

Detailed conditions and antibodies used in flow cytometry analysis are described in the Supplemental Experimental Procedures

Gating Strategy

Gating strategy for the identification of human MDSCs, neutrophils, and monocytes is described in the Supplemental Experimental Procedures.

Histopathological Analysis

Histopathological analysis was performed on BM and spleens from WT, *Rorc1*$^{-/-}$, and chimeric mice on sections routinely stained with H&E. Single- and double-marker immunohistochemistry on mouse and human tissue specimens were performed as previously reported (Tripodo et al., 2012) and are described in detail in the Supplemental Experimental Procedures.

Confocal Microscopy

Confocal Microscopy was performed as previously reported (Moalli et al., 2010) and as described in the Supplemental Experimental Procedures.

Statistics

Statistical significance was determined by a two-tailed Student's t test (*$p < 0.05$, ** $p < 0.01$, *** $p < 0.001$).

SUPPLEMENTAL INFORMATION

Supplemental Information includes Supplemental Experimental Procedures and six figures and can be found with this article online at http://dx.doi.org/10.1016/j.ccell.2015.07.006.

AUTHOR CONTRIBUTIONS

L.S. and A.S. conceived the ideas and designed the experiments. L.S., S.S., F.M.C., G.S., S.M., M.G.T., C.P., A.A., S.T., A.D., F.Z., and C.T. performed the experiments. L.S., S.S., C.T., A.M.C., and A.S. analyzed the data. L.S. and A.S. wrote the paper.

ACKNOWLEDGMENTS

This work was supported by Associazione Italiana Ricerca sul Cancro (AIRC; Program Innovative Tools for Cancer Risk Assessment and Diagnosis, 5 per mille number 12162 and IG number 2014-15585), Fondazione Cariplo, and Ministero Università Ricerca (MIUR).

Received: September 30, 2014
Revised: April 9, 2015
Accepted: July 21, 2015
Published: August 10, 2015

REFERENCES

Akagi, T., Saitoh, T., O'Kelly, J., Akira, S., Gombart, A.F., and Koeffler, H.P. (2008). Impaired response to GM-CSF and G-CSF, and enhanced apoptosis in C/EBPbeta-deficient hematopoietic cells. Blood *111*, 2999–3004.

Auffray, C., Sieweke, M.H., and Geissmann, F. (2009). Blood monocytes: development, heterogeneity, and relationship with dendritic cells. Annu. Rev. Immunol. *27*, 669–692.

Chow, A., Lucas, D., Hidalgo, A., Méndez-Ferrer, S., Hashimoto, D., Scheiermann, C., Battista, M., Leboeuf, M., Prophete, C., van Rooijen, N., et al. (2011). Bone marrow CD169+ macrophages promote the retention of hematopoietic stem and progenitor cells in the mesenchymal stem cell niche. J. Exp. Med. *208*, 261–271.

Coffelt, S.B., Kersten, K., Doornebal, C.W., Weiden, J., Vrijland, K., Hau, C.S., Verstegen, N.J., Ciampricotti, M., Hawinkels, L.J., Jonkers, J., and de Visser, K.E. (2015). IL-17-producing γδ T cells and neutrophils conspire to promote breast cancer metastasis. Nature *522*, 345–348.

Croker, B.A., Metcalf, D., Robb, L., Wei, W., Mifsud, S., DiRago, L., Cluse, L.A., Sutherland, K.D., Hartley, L., Williams, E., et al. (2004). SOCS3 is a critical physiological negative regulator of G-CSF signaling and emergency granulopoiesis. Immunity *20*, 153–165.

Friedman, A.D. (2007). Transcriptional control of granulocyte and monocyte development. Oncogene *26*, 6816–6828.

Gabrilovich, D.I., Ostrand-Rosenberg, S., and Bronte, V. (2012). Coordinated regulation of myeloid cells by tumours. Nat. Rev. Immunol. *12*, 253–268.

Gerbal-Chaloin, S., Iankova, I., Maurel, P., and Daujat-Chavanieu, M. (2013). Nuclear receptors in the cross-talk of drug metabolism and inflammation. Drug Metab. Rev. *45*, 122–144.

Gordy, C., Pua, H., Sempowski, G.D., and He, Y.W. (2011). Regulation of steady-state neutrophil homeostasis by macrophages. Blood *117*, 618–629.

Goren, I., Allmann, N., Yogev, N., Schürmann, C., Linke, A., Holdener, M., Waisman, A., Pfeilschifter, J., and Frank, S. (2009). A transgenic mouse model of inducible macrophage depletion: effects of diphtheria toxin-driven lysozyme M-specific cell lineage ablation on wound inflammatory, angiogenic, and contractive processes. Am. J. Pathol. *175*, 132–147.

Gray, E.E., Suzuki, K., and Cyster, J.G. (2011). Cutting edge: Identification of a motile IL-17-producing gammadelta T cell population in the dermis. J. Immunol. *186*, 6091–6095.

Guo, R.F., and Ward, P.A. (2005). Role of C5a in inflammatory responses. Annu. Rev. Immunol. *23*, 821–852.

Guy, C.T., Cardiff, R.D., and Muller, W.J. (1992). Induction of mammary tumors by expression of polyomavirus middle T oncogene: a transgenic mouse model for metastatic disease. Mol. Cell. Biol. *12*, 954–961.

Figure 8. Reciprocal Negative Regulation of Monocytes/Macrophages and Granulocytes in Cancer-Associated Inflammation

(A) Mean counts ± SEM of CD115- and RORC1-expressing F4/80$^+$ macrophages in the MN/MCA1 tissue from untreated (isotype IgG control) and anti-CSFR1-treated tumor-bearing WT mice.

(B) Mean counts ± SEM of RORC1$^+$ and RORC1$^-$ M-MDSC and PMN-MDSC subsets.

(C) Mean fluorescence intensity (MFI) ± SEM for CD16/CD32 and C5aR expression in PMN-MDSCs in MN/MCA1 from WT mice treated with isotype IgG or ant-CSFR1 antibody.

(A–C) Statistical analysis: *$p < 0.05$, **$p < 0.01$, ***$p < 0.001$; n = 3 (Student's t test).

(D) FACS analysis of RORC1 expression levels in Ly6G^{high} and Ly6G^{low} granulocytes and in F4/80$^+$/CD115$^+$ macrophages.

(E) FACS dot plots for granulocyte (A), monocyte/macrophage (C), and macrophage (D) progenitor subsets in BM and spleen from one representative MN/MCA1-bearing WT mouse treated with IgG isotype and one treated with anti-CSFR1 antibody, both with AD, are shown. The mean ± SD of five mice/experimental group is shown (t test, *$p < 0.05$; n = 5). Statistical analysis: *$p < 0.05$, **$p < 0.01$, ***$p < 0.001$ (Student's t test).

(F) Total CD4$^+$ and CD4$^+$IFN-γ$^+$ and total F4/80$^+$ and F4/80$^+$TNF-α$^+$ subsets in MN/MCA1 tumors from tumor-bearing mice treated with isotype control antibody (white bar) or anti-G-CSF antibody (black bars). The mean ± SEM of six mice/experimental group is shown. Statistical analysis: *$p < 0.05$, **$p < 0.01$, ***$p < 0.001$ (Student's t test).

See also Figure S6.

Harrington, L.E., Hatton, R.D., Mangan, P.R., Turner, H., Murphy, T.L., Murphy, K.M., and Weaver, C.T. (2005). Interleukin 17-producing CD4+ effector T cells develop via a lineage distinct from the T helper type 1 and 2 lineages. Nat. Immunol. *6*, 1123–1132.

Hirai, H., Zhang, P., Dayaram, T., Hetherington, C.J., Mizuno, S., Imanishi, J., Akashi, K., and Tenen, D.G. (2006). C/EBPbeta is required for 'emergency' granulopoiesis. Nat. Immunol. *7*, 732–739.

Hogarth, P.M. (2002). Fc receptors are major mediators of antibody based inflammation in autoimmunity. Curr. Opin. Immunol. *14*, 798–802.

Hueber, A.J., Asquith, D.L., Miller, A.M., Reilly, J., Kerr, S., Leipe, J., Melendez, A.J., and McInnes, I.B. (2010). Mast cells express IL-17A in rheumatoid arthritis synovium. J. Immunol. *184*, 3336–3340.

Hume, D.A., and MacDonald, K.P. (2012). Therapeutic applications of macrophage colony-stimulating factor-1 (CSF-1) and antagonists of CSF-1 receptor (CSF-1R) signaling. Blood *119*, 1810–1820.

Ivanov, I.I., McKenzie, B.S., Zhou, L., Tadokoro, C.E., Lepelley, A., Lafaille, J.J., Cua, D.J., and Littman, D.R. (2006). The orphan nuclear receptor RORgammat directs the differentiation program of proinflammatory IL-17+ T helper cells. Cell *126*, 1121–1133.

Iwakura, Y., Ishigame, H., Saijo, S., and Nakae, S. (2011). Functional specialization of interleukin-17 family members. Immunity *34*, 149–162.

Jin, F., Li, Y., Ren, B., and Natarajan, R. (2011). PU.1 and C/EBP(alpha) synergistically program distinct response to NF-kappaB activation through establishing monocyte specific enhancers. Proc. Natl. Acad. Sci. USA *108*, 5290–5295.

Kojetin, D.J., and Burris, T.P. (2014). REV-ERB and ROR nuclear receptors as drug targets. Nat. Rev. Drug Discov. *13*, 197–216.

Kreisel, D., Sugimoto, S., Tietjens, J., Zhu, J., Yamamoto, S., Krupnick, A.S., Carmody, R.J., and Gelman, A.E. (2011). Bcl3 prevents acute inflammatory lung injury in mice by restraining emergency granulopoiesis. J. Clin. Invest. *121*, 265–276.

Larghi, P., Porta, C., Riboldi, E., Totaro, M.G., Carraro, L., Orabona, C., and Sica, A. (2012). The p50 subunit of NF-κB orchestrates dendritic cell lifespan and activation of adaptive immunity. PLoS ONE *7*, e45279.

Liu, B., Tan, W., Barsoum, A., Gu, X., Chen, K., Huang, W., Ramsay, A., Kolls, J.K., and Schwarzenberger, P. (2010). IL-17 is a potent synergistic factor with GM-CSF in mice in stimulating myelopoiesis, dendritic cell expansion, proliferation, and functional enhancement. Exp. Hematol. *38*, 877–884.e1.

Mantovani, A., and Sica, A. (2010). Macrophages, innate immunity and cancer: balance, tolerance, and diversity. Curr. Opin. Immunol. *22*, 231–237.

Mantovani, A., Cassatella, M.A., Costantini, C., and Jaillon, S. (2011). Neutrophils in the activation and regulation of innate and adaptive immunity. Nat. Rev. Immunol. *11*, 519–531.

Marigo, I., Bosio, E., Solito, S., Mesa, C., Fernandez, A., Dolcetti, L., Ugel, S., Sonda, N., Bicciato, S., Falisi, E., et al. (2010). Tumor-induced tolerance and immune suppression depend on the C/EBPbeta transcription factor. Immunity *32*, 790–802.

Metcalf, D. (2008). Hematopoietic cytokines. Blood *111*, 485–491.

Moalli, F., Doni, A., Deban, L., Zelante, T., Zagarella, S., Bottazzi, B., Romani, L., Mantovani, A., and Garlanda, C. (2010). Role of complement and Fcgamma receptors in the protective activity of the long pentraxin PTX3 against Aspergillus fumigatus. Blood *116*, 5170–5180.

Peranzoni, E., Zilio, S., Marigo, I., Dolcetti, L., Zanovello, P., Mandruzzato, S., and Bronte, V. (2010). Myeloid-derived suppressor cell heterogeneity and subset definition. Curr. Opin. Immunol. *22*, 238–244.

Porta, C., Rimoldi, M., Raes, G., Brys, L., Ghezzi, P., Di Liberto, D., Dieli, F., Ghisletti, S., Natoli, G., De Baetselier, P., et al. (2009). Tolerance and M2 (alternative) macrophage polarization are related processes orchestrated by p50 nuclear factor kappaB. Proc. Natl. Acad. Sci. USA *106*, 14978–14983.

Qian, B.Z., and Pollard, J.W. (2010). Macrophage diversity enhances tumor progression and metastasis. Cell *141*, 39–51.

Rachitskaya, A.V., Hansen, A.M., Horai, R., Li, Z., Villasmil, R., Luger, D., Nussenblatt, R.B., and Caspi, R.R. (2008). Cutting edge: NKT cells constitutively express IL-23 receptor and RORgammat and rapidly produce IL-17 upon receptor ligation in an IL-6-independent fashion. J. Immunol. *180*, 5167–5171.

Ries, C.H., Cannarile, M.A., Hoves, S., Benz, J., Wartha, K., Runza, V., Rey-Giraud, F., Pradel, L.P., Feuerhake, F., Klaman, I., et al. (2014). Targeting tumor-associated macrophages with anti-CSF-1R antibody reveals a strategy for cancer therapy. Cancer Cell *25*, 846–859.

Sawa, S., Cherrier, M., Lochner, M., Satoh-Takayama, N., Fehling, H.J., Langa, F., Di Santo, J.P., and Eberl, G. (2010). Lineage relationship analysis of RORgammat+ innate lymphoid cells. Science *330*, 665–669.

Schwarzenberger, P., Huang, W., Ye, P., Oliver, P., Manuel, M., Zhang, Z., Bagby, G., Nelson, S., and Kolls, J.K. (2000). Requirement of endogenous stem cell factor and granulocyte-colony-stimulating factor for IL-17-mediated granulopoiesis. J. Immunol. *164*, 4783–4789.

Sica, A., and Bronte, V. (2007). Altered macrophage differentiation and immune dysfunction in tumor development. J. Clin. Invest. *117*, 1155–1166.

Sica, A., Saccani, A., Bottazzi, B., Polentarutti, N., Vecchi, A., van Damme, J., and Mantovani, A. (2000). Autocrine production of IL-10 mediates defective IL-12 production and NF-kappa B activation in tumor-associated macrophages. J. Immunol. *164*, 762–767.

Sinha, P., Chornoguz, O., Clements, V.K., Artemenko, K.A., Zubarev, R.A., and Ostrand-Rosenberg, S. (2011). Myeloid-derived suppressor cells express the death receptor Fas and apoptose in response to T cell-expressed FasL. Blood *117*, 5381–5390.

Stutman, O. (1974). Tumor development after 3-methylcholanthrene in immunologically deficient athymic-nude mice. Science *183*, 534–536.

Sun, Z., Unutmaz, D., Zou, Y.R., Sunshine, M.J., Pierani, A., Brenner-Morton, S., Mebius, R.E., and Littman, D.R. (2000). Requirement for RORgamma in thymocyte survival and lymphoid organ development. Science *288*, 2369–2373.

Taylor, P.R., Roy, S., Leal, S.M., Jr., Sun, Y., Howell, S.J., Cobb, B.A., Li, X., and Pearlman, E. (2014). Activation of neutrophils by autocrine IL-17A-IL-17RC interactions during fungal infection is regulated by IL-6, IL-23, RORγt and dectin-2. Nat. Immunol. *15*, 143–151.

Toomer, K.H., and Chen, Z. (2014). Autoimmunity as a double agent in tumor killing and cancer promotion. Front. Immunol. *5*, 116.

Torroella-Kouri, M., Silvera, R., Rodriguez, D., Caso, R., Shatry, A., Opiela, S., Ilkovitch, D., Schwendener, R.A., Iragavarapu-Charyulu, V., Cardentey, Y., et al. (2009). Identification of a subpopulation of macrophages in mammary tumor-bearing mice that are neither M1 nor M2 and are less differentiated. Cancer Res. *69*, 4800–4809.

Tripodo, C., Sangaletti, S., Guarnotta, C., Piccaluga, P.P., Cacciatore, M., Giuliano, M., Franco, G., Chiodoni, C., Sciandra, M., Miotti, S., et al. (2012). Stromal SPARC contributes to the detrimental fibrotic changes associated with myeloproliferation whereas its deficiency favors myeloid cell expansion. Blood *120*, 3541–3554.

Ueha, S., Shand, F.H., and Matsushima, K. (2011). Myeloid cell population dynamics in healthy and tumor-bearing mice. Int. Immunopharmacol. *11*, 783–788.

Ulich, T.R., del Castillo, J., and Souza, L. (1988). Kinetics and mechanisms of recombinant human granulocyte-colony stimulating factor-induced neutrophilia. Am. J. Pathol. *133*, 630–638.

Winkler, I.G., Sims, N.A., Pettit, A.R., Barbier, V., Nowlan, B., Helwani, F., Poulton, I.J., van Rooijen, N., Alexander, K.A., Raggatt, L.J., and Lévesque, J.P. (2010). Bone marrow macrophages maintain hematopoietic stem cell (HSC) niches and their depletion mobilizes HSCs. Blood *116*, 4815–4828.

Wittke, A., Weaver, V., Mahon, B.D., August, A., and Cantorna, M.T. (2004). Vitamin D receptor-deficient mice fail to develop experimental allergic asthma. J. Immunol. *173*, 3432–3436.

Wu, P., Wu, D., Ni, C., Ye, J., Chen, W., Hu, G., Wang, Z., Wang, C., Zhang, Z., Xia, W., et al. (2014). γδT17 cells promote the accumulation and expansion of myeloid-derived suppressor cells in human colorectal cancer. Immunity *40*, 785–800.

Yang, X.O., Pappu, B.P., Nurieva, R., Akimzhanov, A., Kang, H.S., Chung, Y., Ma, L., Shah, B., Panopoulos, A.D., Schluns, K.S., et al. (2008). T helper 17 lineage differentiation is programmed by orphan nuclear receptors ROR alpha and ROR gamma. Immunity *28*, 29–39.

Zamarron, B.F., and Chen, W. (2011). Dual roles of immune cells and their factors in cancer development and progression. Int. J. Biol. Sci. *7*, 651–658.

Zhang, H., Nguyen-Jackson, H., Panopoulos, A.D., Li, H.S., Murray, P.J., and Watowich, S.S. (2010). STAT3 controls myeloid progenitor growth during emergency granulopoiesis. Blood *116*, 2462–2471.

Zhu, X., Mulcahy, L.A., Mohammed, R.A., Lee, A.H., Franks, H.A., Kilpatrick, L., Yilmazer, A., Paish, E.C., Ellis, I.O., Patel, P.M., and Jackson, A.M. (2008). IL-17 expression by breast-cancer-associated macrophages: IL-17 promotes invasiveness of breast cancer cell lines. Breast Cancer Res. *10*, R95.

Zhuang, Y., Peng, L.S., Zhao, Y.L., Shi, Y., Mao, X.H., Chen, W., Pang, K.C., Liu, X.F., Liu, T., Zhang, J.Y., et al. (2012). CD8(+) T cells that produce interleukin-17 regulate myeloid-derived suppressor cells and are associated with survival time of patients with gastric cancer. Gastroenterology *143*, 951–962.e8.